crystals

MDPI

Article

Influence of Superplasticizers on the Diffusion-Controlled Synthesis of Gypsum Crystals

F. Kakar *, C. Pritzel, T. Kowald and M. S. Killian *

Chemistry and Structure of Novel Materials, University of Siegen, 57076 Siegen, Germany; pritzel@chemie.uni-siegen.de (C.P.); kowald@chemie.uni-siegen.de (T.K.)
* Correspondence: faiz.kakar@uni-siegen.de (F.K.); manuela.killian@uni-siegen.de (M.S.K.)

Abstract

Gypsum ($CaSO_4 \cdot 2H_2O$) crystallization underpins numerous industrial processes, yet its response to chemical admixtures remains incompletely understood. This study investigates diffusion-controlled crystal growth in a coaxial test tube system to evaluate how three Sika® ViscoCrete® superplasticizers—430P, 111P, and 120P—affect nucleation, growth kinetics, morphology, and thermal behavior. The superplasticizers, selected for their surface-active properties, were hypothesized to influence crystallization via interfacial interactions. Ion diffusion was maintained quasi-steadily for 12 weeks, with crystal evolution tracked weekly by macro-photography; scanning electron microscopy and thermogravimetric/differential scanning were performed at the final stage. All admixtures delayed nucleation in a concentration-dependent manner. Lower dosages (0.5–1.0 wt%) yielded platy-to-prismatic morphologies and higher dehydration enthalpies, indicating more ordered lattice formation. In contrast, higher dosages (1.5–2.0 wt%) produced denser, irregular crystals and shifted dehydration to lower temperatures, suggesting structural defects or increased hydration. Among the additives, 120P showed the strongest inhibitory effect, while 111P at 0.5 wt% resulted in the most uniform crystals. These results demonstrate that ViscoCrete® superplasticizers can modulate gypsum crystallization and thermal properties.

Keywords: gypsum crystallization; superplasticizer; crystal growth; morphology; controlled diffusion

check for updates

Academic Editor: Jesús Sanmartín-Matalobos

Received: 30 June 2025
Revised: 25 July 2025
Accepted: 31 July 2025
Published: 31 July 2025

Citation: Kakar, F.; Pritzel, C.; Kowald, T.; Killian, M.S. Influence of Superplasticizers on the Diffusion-Controlled Synthesis of Gypsum Crystals. *Crystals* **2025**, *15*, 709. https://doi.org/10.3390/cryst15080709

Copyright: © 2025 by the authors. Licensee MDPI, Basel, Switzerland. This article is an open access article distributed under the terms and conditions of the Creative Commons Attribution (CC BY) license (https://creativecommons.org/licenses/by/4.0/).

1. Introduction

Gypsum ($CaSO_4 \cdot 2H_2O$) is one of the most versatile and widely used materials in construction and various industrial applications, owing to its unique physical and chemical properties. It finds extensive usage not only in conventional building materials but also in casting, medical formulations, agriculture, and specialized manufacturing processes [1–4]. The crystallization behavior of gypsum, especially under controlled conditions such as slow ion diffusion in static or semi-static environments, plays a fundamental role in determining its final morphology, thermal stability, microstructure, and consequently, its mechanical and durability properties [5–9]. Understanding and controlling gypsum crystallization is critical for optimizing its performance in diverse applications. However, the influence of chemical admixtures—particularly superplasticizers—on gypsum crystal growth remains an area of ongoing research especially in chemically aggressive environments such as phosphoric or sulfuric acid media [10]. Superplasticizers, especially polycarboxylate-based polymers, have been increasingly used in cementitious systems to enhance workability and reduce water demand, without sacrificing strength [11,12]. These additives modulate

key crystallization mechanisms, including nucleation rate, crystal growth kinetics, and the organization of crystal morphology, which ultimately affect the microstructural and macroscopic properties of gypsum materials [13–18]. Recent advances in polymer chemistry have led to the synthesis of various superplasticizer classes, such as triblock polycarboxylates, sulfonated polystyrenes, and novel copolymers, each with specific molecular architectures designed to optimize dispersion and interaction with gypsum particles [19–21]. These materials improve particle dispersion, refine the microstructure, and significantly enhance the mechanical strength and long-term durability of gypsum composites, while also contributing to improved water resistance in the final product [3,14,22,23]. Moreover, the chemical composition and dosage of these superplasticizers critically influence hydration reactions and microstructural development during gypsum setting and hardening [4,24–26]. This study specifically examines the effects of three different commercially available Sika® ViscoCrete® superplasticizers—430P, 111P, and 120P (Sika AG, Baar, Switzerland)—on gypsum crystallization using a diffusion-controlled experimental setup. These superplasticizers were obtained from Sika AG, Baar, Switzerland.

By investigating varying concentrations of these admixtures, this study aims to elucidate their impact on gypsum's morphological evolution, thermal behavior, and crystal morphology under quasi-equilibrium conditions [6,27]. Such understanding is vital for tuning gypsum properties like setting time, mechanical performance, and thermal stability, which are essential for enhancing the material's practical applications in construction and building technologies. As demonstrated in previous studies on phosphorus gypsum systems, specific chemical admixtures can significantly affect these properties by modifying hydration kinetics, improving workability, and enhancing strength development [28–30]. Characterization techniques such as Scanning Electron Microscopy (SEM), Thermogravimetric Analysis (TGA), and Differential Scanning Calorimetry (DSC) are utilized to assess the microstructural and thermal modifications induced by superplasticizer incorporation. In the course of this study, it was observed that lower concentrations of superplasticizer (0.5–1.0 wt%) tend to promote the formation of well-ordered, layered gypsum crystals with higher dehydration enthalpies, whereas higher concentrations (1.5–2.0 wt%) result in denser but less well-defined crystal structures exhibiting reduced thermal stability. These structural variations correlate with corresponding changes in thermal properties, highlighting the critical role of superplasticizer dosage in directing gypsum crystal growth and influencing overall material performance [31–33]. These additives not only improve mechanical strength but also enhance durability and water resistance, which are critical for the longevity of gypsum-based construction materials [34–37]. Beyond improving mechanical and thermal characteristics, the integration of recycled pozzolanic materials and other solid wastes with gypsum and superplasticizers has demonstrated promising advances in sustainability and material functionality. These composites show enhanced mechanical properties and environmental benefits, supporting the growing emphasis on eco-friendly construction materials [29,35,36]. Additive manufacturing techniques using gypsum and polymer granulates have also opened new horizons for lightweight and thermally efficient building components [32]. In summary, the strategic use of superplasticizers in gypsum systems offers powerful means to tailor crystal synthesis and final material properties. This research contributes to the fundamental understanding of polymer-mineral interactions during gypsum crystallization and provides a foundation for engineering advanced gypsum-based materials with improved structural integrity, durability, and environmental performance, paving the way toward sustainable building solution [38,39].

2. Experimental

In this study, calcium chloride ($CaCl_2$, 2.2 g) and sodium sulfate (Na_2SO_4, 2.8 g) were used as the starting materials to induce gypsum ($CaSO_4 \cdot 2H_2O$) crystallization via a controlled diffusion process. The calcium chloride used had a molar mass of 110.99 g/mol and the sodium sulfate had a molar mass of 142.04 g/mol. The two salts were placed separately into two test tubes: calcium chloride was introduced into a larger test tube, and sodium sulfate was added to a smaller test tube. The smaller test tube was then carefully inserted into the larger one, ensuring that no mixing of the two solid materials occurred at this stage. Following this, deionized water was slowly added into both test tubes using a syringe. The addition was performed gently and gradually to prevent any premature mixing or disturbance of the salt layers. This careful setup ensured a stable starting condition for the diffusion-driven crystallization process. Once both test tubes were completely filled with water, the mouth of the larger test tube was sealed with a test tube cap. To further secure the closure and prevent evaporation or contamination, the cap was tightly wrapped with Parafilm. The system was then placed under ambient laboratory conditions at 23 ± 1 °C, relative humidity of approximately 50%, and under standard indoor lighting without direct sunlight, and left undisturbed to allow the diffusion-driven reaction to proceed. As part of the investigation into the effects of chemical admixtures on gypsum crystallization, several types of superplasticizers were initially screened. Among them, three representative products from the Sika® ViscoCrete® series were selected for detailed evaluation: Sika® ViscoCrete® 430P, Sika® ViscoCrete® 111P, and Sika® ViscoCrete® 120P. The three superplasticizers used in this study (SP-430, SP-111, and SP-120) are modified polycarboxylate ether (PCE) powders with similar base chemistry but differences in their molecular architecture, charge density, and adsorption kinetics. According to the manufacturer, all three products are formaldehyde- and ammonia-free, have low chloride content (≤0.1%), and comparable pH and bulk density values, yet their performance differences are attributed to variations in side-chain optimization and surface charge density The key characteristics of these three superplasticizers, as reported in the manufacturer's datasheets, are presented in Table 1. For each selected superplasticizer, four aqueous solutions were prepared at concentrations of 0.5%, 1%, 1.5%, and 2% (*w*/*w*). These concentrations were calculated based on the theoretical gypsum yield from the initial amounts of calcium chloride (2.2 g) and sodium sulfate (2.8 g). All superplasticizers were initially provided in fine powder form and were dissolved in deionized water at 23 ± 1 °C under magnetic stirring. Stirring continued until complete dissolution was achieved and the solutions appeared clear and homogeneous.

The experimental procedure for the superplasticizer-containing systems followed the same protocol as the reference setup. Each solution was introduced into the respective test tubes using a syringe to carefully fill both the inner and outer tubes with minimal disturbance. The larger tube was then sealed with a cap and wrapped with Parafilm to preserve the internal environment. All samples were maintained under identical ambient conditions to ensure consistency and comparability of the crystal growth results. Two types of coaxial test tubes with different dimensions were employed to serve as the reaction environment for gypsum crystallization (Figure 1a). This coaxial configuration was deliberately designed to create a static, undisturbed setting that facilitates the gradual diffusion of ions and supports the natural and orderly crystallization of gypsum within the annular space between the two tubes. This setup enabled precise regulation of the diffusion rate and provided a controlled platform to evaluate the influence of chemical admixtures. A schematic illustration of the overall experimental setup and the initial stages of gypsum crystal formation via the reaction between Na_2SO_4 and $CaCl_2$ in deionized or superplasticizer-containing solution is shown in Figure 1b.

Table 1. Key physicochemical properties of the three superplasticizers (SP-430, SP-111, and SP-120) as reported by the manufacturer's datasheets.

Property	SP-430	SP-111	SP-120
Composition	Modified polycarboxylate (PCE)	Modified polycarboxylate (PCE)	Modified polycarboxylate (PCE)
Appearance/Color	White to yellowish powder	White to yellowish powder	White to yellowish powder
Bulk density (g/cm^3)	~0.51–0.61	~0.60	~0.55
pH (40% solution)	~4.0–5.0	~4.0	~4.0
Total chloride content	≤0.1%	≤0.1%	≤0.1%
Storage conditions	Dry, ≤30 °C, protect from sunlight	Dry, ≤30 °C, protect from sunlight	Dry, ≤30 °C, protect from sunlight
Shelf life	24 months	24 months	24 months

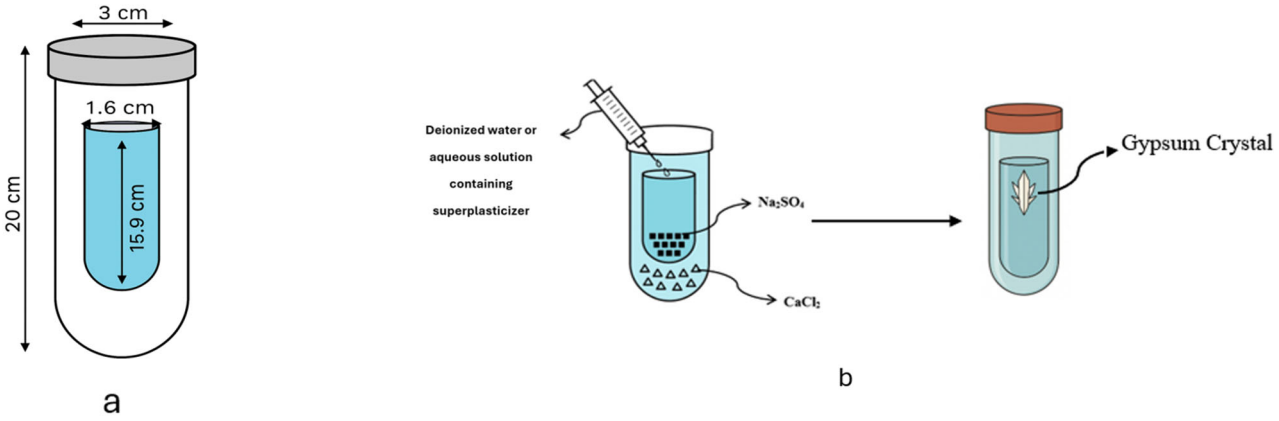

Figure 1. (**a**) Schematic representation of the coaxial test tube setup used for gypsum crystallization, showing the inner and outer tubes with respective dimensions. (**b**) Illustration of the initial steps of gypsum crystal formation through the reaction of Na_2SO_4 and $CaCl_2$ in either deionized water or a superplasticizer-containing solution.

2.1. Photographic Monitoring of the Crystal Growth Process Was Carried out on a Weekly Basis over a Period of Four Months

Images were systematically captured to document the morphological development of gypsum crystals under both reference conditions and in the presence of the different superplasticizers at their respective concentrations (0.5%, 1%, 1.5%, and 2%). All photographs were taken using an iPhone 14 Pro Max (Apple Inc., Cupertino, CA, USA), which features a triple-lens camera system including a 12 MP wide (f/1.5), ultra-wide (f/1.8), and telephoto (f/2.8) lens. Standardized lighting conditions and camera distance were maintained throughout the experiment to ensure consistent image quality and comparability. The high-resolution images obtained enabled detailed visual tracking of crystal morphology, nucleation patterns, and growth evolution. This longitudinal documentation facilitated a comparative analysis of crystal growth behavior influenced by the presence and concentration of various Sika® ViscoCrete® admixtures. At the end of the four months, all test tubes were carefully opened, and the formed gypsum crystals were collected. The collection process involved first decanting or discarding the aqueous solution from each test tube, taking care not to disturb the crystal structures. The remaining crystals were then gently transferred into glass containers. To remove residual moisture and bound water, the collected crystals were placed in a laboratory oven set at 40 °C for a duration of 4 h.

2.2. Scanning Electron Microscopy (SEM) of Gypsum Crystals

The surface morphology of the synthesized gypsum crystals was examined using a FEI FEG Quanta 240 Environmental Scanning Electron Microscope (ESEM). Imaging was performed in low vacuum mode (~100 Pa) at an accelerating voltage of 30 kV, with a working distance of approximately 10 mm. Backscattered electron detection (BSED) was employed to enhance surface topography contrast. Before imaging, the gypsum crystals were oven-dried at 40 °C for 4 h to remove residual moisture and then affixed to aluminum sample holders using conductive carbon tape to ensure proper electrical contact and mechanical stability. No additional conductive coating was applied, as the low-vacuum mode of the ESEM allowed imaging of the non-conductive gypsum crystals without sputter coating. SEM images were captured at various magnifications to observe both fine surface details and overall morphological characteristics.

2.3. X-Ray Diffraction (XRD) Analysis of Reference Gypsum Crystals

The reference gypsum crystals were analyzed by X-ray diffraction (XRD) using a Panalytical X'Pert Pro PW 3040/60 powder diffractometer (Malvern Panalytical Ltd., Malvern, UK).

2.4. Thermal Characterization via TGA-DSC Analysis

Thermal analysis was conducted using a STA 449 C Jupiter analyzer (NETZSCH, Selb, Germany) equipped with TGA-DSC capabilities to investigate the thermal behavior of gypsum crystals with and without superplasticizer additives. Approximately 40 mg of each sample was placed in a Pt-Rh crucible and subjected to a multi-segment thermal program ranging from room temperature (25 °C) to 1000 °C at a heating rate of 10 K/min. The experiment was carried out under a dynamic atmosphere featuring separate gas inlets: nitrogen (20 mL/min × 2) was introduced into the oven chamber to directly interact with the sample, while argon (20 mL/min) was independently supplied through the balance compartment, functioning as a protective gas for the weighing system. This separation of gas pathways ensured a stable thermal environment and protected the balance from thermal and chemical disturbances. All gas flow rates were precisely controlled using MFCs (Mass Flow Controllers), and purge conditions were maintained throughout the measurement. Data acquisition and correction were performed using Proteus® software Version 6.1.0 (02.06.2015), enabling high-precision monitoring of mass loss and heat flow. This protocol allowed for a comprehensive assessment of the thermal stability, dehydration behavior, and phase transitions of the gypsum samples. Prior to thermal analysis, the gypsum crystal samples were rinsed with deionized water to remove any residual mother liquor or loosely bound superplasticizer and then dried at 40 °C for 4 h to minimize surface moisture. It should be noted that different analytical steps (such as SEM imaging and thermal analysis) were performed on separate samples selected from the synthesized crystals. Thus, all characterizations were not conducted on a single crystal but on multiple samples. A general schematic overview of the experimental workflow—including sample preparation, crystal growth monitoring, collection, drying, and subsequent analysis—is presented in Figure 2.

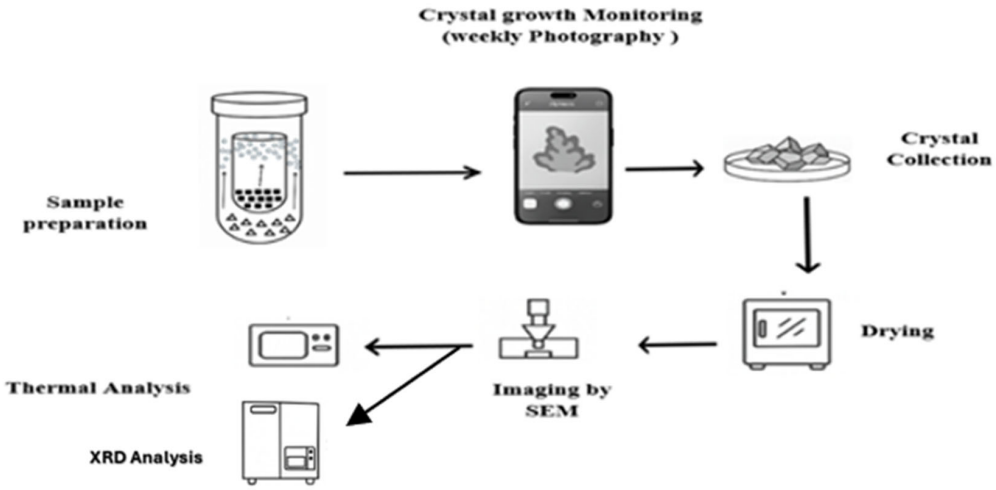

Figure 2. General schematic representation of the experimental workflow, including sample preparation, photographic monitoring of crystal growth, crystal collection and drying, SEM imaging, XRD analysis and thermal analysis.

3. Result and Discussion

3.1. Kinetics and Morphology of Diffusion-Controlled Gypsum Crystal Growth in Aqueous Solution over 12 Weeks

The process of gypsum ($CaSO_4 \cdot 2H_2O$) crystal growth in aqueous solution over a 12-week period is clearly observable across the four provided images in Figure 3 and can be analyzed using fundamental crystallization principles.

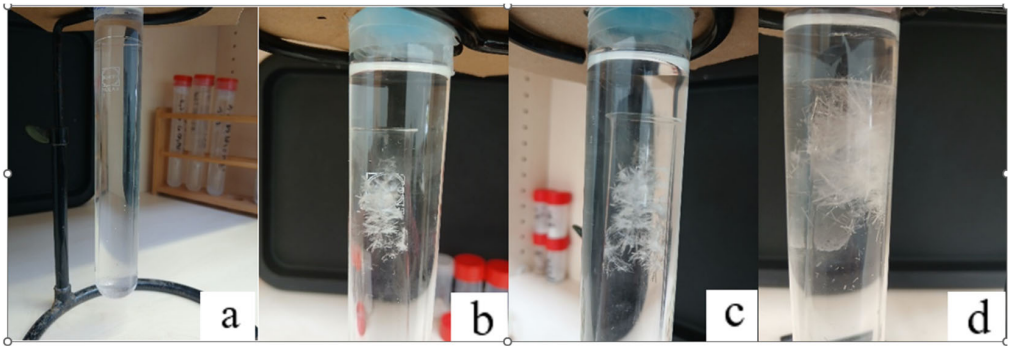

Figure 3. Visual progression of gypsum crystal growth over 12 weeks: (**a**) Week 1—clear, no crystallization; (**b**) Week 3—initial needle-like crystals; (**c**) Week 4—radial crystal growth; (**d**) Week 12—dense fibrous crystals.

In week 1, the solution remains completely clear and colorless, indicating that no crystallization has occurred yet. This suggests that the system is in a state of supersaturation, but nucleation has not yet been initiated, likely due to insufficient time or suboptimal conditions. By week 3, the first signs of crystal formation become visible as fine, needle-like structures along the inner wall of the test tube. This marks the beginning of the nucleation stage, where a few stable crystals begin to grow. The sparse and isolated nature of these crystals reflects a slow and controlled growth environment. By week 4, the crystals had grown larger and become more numerous, showing a more pronounced and somewhat radial arrangement. This indicates the transition into the crystal growth stage, where the existing nuclei continue to grow as ions from the solution are deposited onto them. At this point, secondary nucleation is minimal, and crystal enlargement dominates. Finally, in week 12, the crystals appear dense, clustered, and well-developed, with a visibly fibrous and voluminous texture. This suggests that the system has reached equilibrium, where

the concentration of dissolved ions has decreased to the solubility limit, effectively halting further significant growth. Overall, the observed progression—from a clear solution to a fully crystallized state—follows the classical crystallization model, including the stages of supersaturation, nucleation, crystal growth, and saturation equilibrium. The visual evidence reflects a stable and controlled environment conducive to high-quality crystal development over time.

3.2. Effect of Varying Concentrations of Sika® ViscoCrete® 430P on Early-Stage Gypsum Crystallization in Aqueous Solution

The early-stage crystallization behavior of gypsum ($CaSO_4 \cdot 2H_2O$) after four weeks in the presence of varying concentrations of the superplasticizer Sika® ViscoCrete® 430P was investigated Figure 4. demonstrates a clear concentration-dependent influence on nucleation and crystal growth. At 0.5%, a distinct and well-developed gypsum crystal is observed, indicating that nucleation proceeds relatively unhindered. At 1%, a more clustered and controlled crystallization pattern appears, suggesting moderate inhibition of ion diffusion and spatial redistribution of crystal nuclei. At 1.5%, the crystal growth becomes more elongated and filamentous, reflecting diffusion-limited conditions and directional growth likely influenced by the presence of the polymer. At 2%, only a single, small, isolated crystal is detected, indicating a significant suppression of both nucleation and growth due to enhanced diffusion control. Overall, Sika® ViscoCrete® 430P acts as an effective diffusion-modulating agent, with increasing concentrations progressively delaying and reducing gypsum crystallization in aqueous solution.

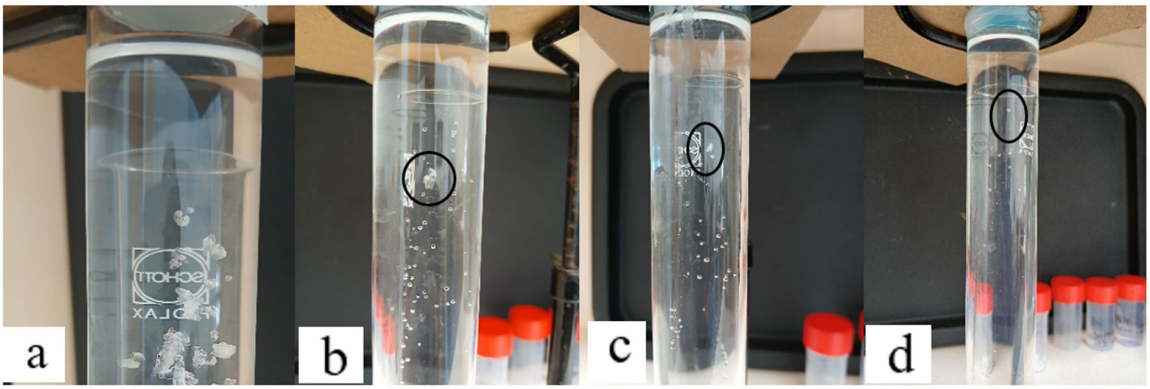

Figure 4. Effect of varying concentrations of Sika® ViscoCrete® 430P on early-stage gypsum ($CaSO_4 \cdot 2H_2O$) crystallization after four weeks: (**a**) 0.5%—distinct and well-developed crystals; (**b**) 1%—clustered and moderately controlled crystallization; (**c**) 1.5%—elongated, filamentous growth; (**d**) 2%—a single small isolated crystal. Increasing concentrations progressively suppress nucleation and crystal growth.

3.3. Concentration-Dependent Effects of Sika® ViscoCrete® 430P on Gypsum Crystal Growth and Morphology After 12 Weeks

After 12 weeks of gypsum synthesis in the presence of various concentrations of the superplasticizer Sika® ViscoCrete® 430P, significant differences were observed, cf. Figure 5, in the growth and morphology of the crystals. At a concentration of 0.5%, the crystals appeared relatively large, transparent, and well-formed, distributed throughout the solution, indicating minimal diffusion inhibition and relatively unrestricted crystal growth. At 1%, the crystals formed as dense aggregates attached to the inner wall of the test tube, suggesting increased primary nucleation but limited volumetric expansion. At 1.5%, the crystals were smaller, more rounded, and more sparsely distributed, indicating a noticeable inhibitory effect of the superplasticizer upon ion diffusion and a reduction in the crystal growth rate. Finally, at 2%, the crystal structures appeared irregular, fine, and highly clus-

tered, reflecting a strong suppression of both nucleation and growth. Overall, increasing concentrations of Sika® ViscoCrete® 430P had a marked influence on the gypsum crystallization process, with the superplasticizer effectively limiting mass transfer and crystal development through surface interactions and diffusion control. These qualitative observations are summarized in Tables 2 and 3, which compares crystal morphology, growth behavior, and sediment characteristics at different concentrations of Sika® ViscoCrete® 430P after 12 weeks of crystallization.

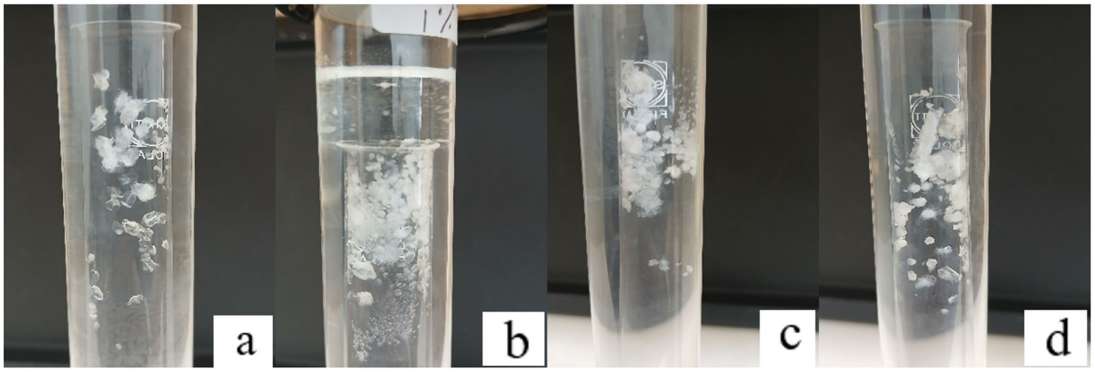

Figure 5. Effect of Sika® ViscoCrete® 430P concentration on gypsum ($CaSO_4 \cdot 2H_2O$) crystal growth and morphology after 12 weeks: (**a**) 0.5%—large, transparent, well-formed crystals; (**b**) 1%—dense aggregates adhering to the tube wall; (**c**) 1.5%—smaller, rounded, sparsely distributed crystals; (**d**) 2%—fine, irregular, and highly clustered crystals. Higher concentrations increasingly inhibit both nucleation and growth through diffusion and surface interaction mechanisms.

Table 2. Summary of observed crystallization stages, crystal morphology, and solution appearance over the 12-week experimental period with Sika® ViscoCrete® 430P addition.

Time	Crystallization Stage	Crystal Observation	Solution Appearance
1st week	Supersaturation (Pre-nucleation)	No visible crystals	Clear and colorless
3rd week	Initial Nucleation	Few distinct crystals begin to appear	Slightly cloudy
4th week	Crystal Growth	Larger, elongated, filamentous or clustered depending on concentration	Moderately cloudy
12th week	Saturation and Final Equilibrium	Morphology dependent on concentration: well-formed at 0.5%, fine/irregular at 2%	Cloudy and dense or soft clusters

Table 3. Summary of the concentration-dependent effects of Sika® ViscoCrete® 430P on gypsum ($CaSO_4 \cdot 2H_2O$) crystal morphology, growth behavior, and sediment characteristics after 12 weeks.

Concentration (%) Sika® ViscoCrete® 430P	Crystal Morphology	Growth Behavior	Sediment Characteristics
0.5%	Distinct, large, transparent, well-formed	Minimal inhibition, unrestricted growth	Distributed, heavy settled crystals
1%	Dense aggregates adhering to wall	Moderate inhibition, limited volumetric growth	Compact clusters, wall-adhered
1.5%	Smaller, rounded, sparsely distributed	Noticeable inhibition, reduced growth rate	Sparse, light fragments
2%	Fine, irregular, highly clustered	Strong suppression of nucleation and growth	Fine, soft powder-like clusters

3.4. Effect of Varying Concentrations of Sika® ViscoCrete® 111P on Early-Stage Gypsum Crystallization in Aqueous Solution

After four weeks of gypsum ($CaSO_4 \cdot 2H_2O$) crystallization in the presence of varying concentrations of the superplasticizer Sika® ViscoCrete® 111P, distinct differences in crystal growth and morphology were observed, cf. Figure 6. At a concentration of 0.5%, the crystals appeared well-formed, elongated, and directionally oriented, indicating that nucleation and growth proceeded with minimal restriction and ion mobility in the solution remained relatively unhindered. At 1%, the crystals were smaller and more compact with poorly defined edges, suggesting a reduction in growth rate due to moderate diffusion inhibition. At 1.5%, only a few small and scattered crystals were visible, reflecting a stronger inhibitory effect of SP-111 on crystal development. Finally, at 2%, the crystals were extremely small, sparse, and incompletely formed, indicating a significant suppression of both nucleation and growth. Overall, increasing the concentration of SP-111 clearly reduced the extent of gypsum crystal formation, highlighting its role as a diffusion-limiting agent and an effective modulator of crystallization kinetics.

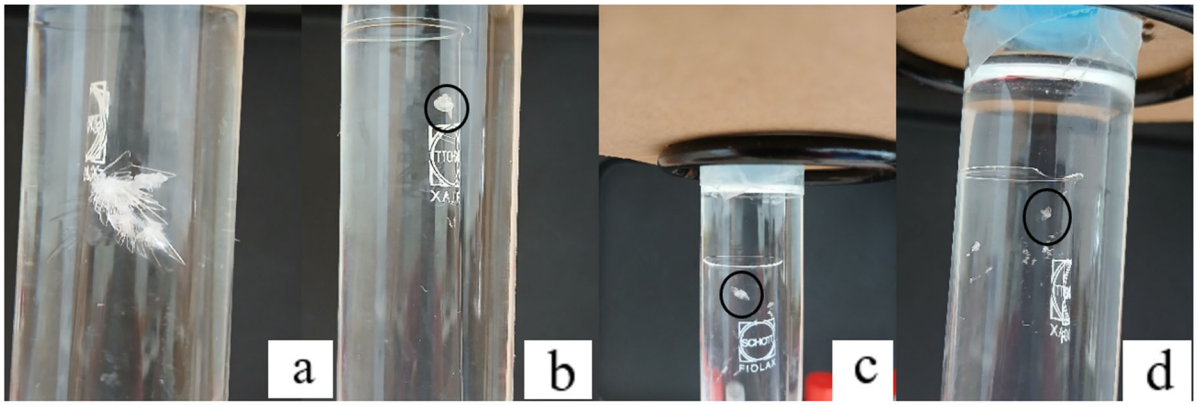

Figure 6. Effect of Sika® ViscoCrete® 111P concentration on gypsum ($CaSO_4 \cdot 2H_2O$) crystal growth and morphology after 4 weeks. (**a**) 0.5%—elongated, well-formed, and directionally oriented crystals, indicating minimal restriction to growth; (**b**) 1%—smaller, compact crystals with poorly defined edges, suggesting moderate inhibition of growth; (**c**) 1.5%—few small and scattered crystals, reflecting stronger suppression of crystal development; (**d**) 2%—extremely small, sparse, and incompletely formed crystals, indicating significant inhibition of both nucleation and growth. Increasing superplasticizer concentration progressively limits crystallization through diffusion restriction and surface interactions.

3.5. Concentration-Dependent Effects of Sika® ViscoCrete® 111P on Gypsum Crystal Growth and Morphology After 12 Weeks

After 12 weeks of gypsum ($CaSO_4 \cdot 2H_2O$) crystallization in the presence of different concentrations of the superplasticizer Sika® ViscoCrete® 111P, significant differences in crystal morphology, size, and sediment quality were observed, cf. Figure 7.

At a concentration of 0.5%, the crystals appeared dense, branched, and structurally well-defined, indicating unrestricted growth and sedimentation due to the weight of fully developed crystals. At 1%, the crystals became smaller, more compact, and exhibited less distinct edges, reflecting a gradual decrease in growth dynamics and the onset of diffusion limitation. At 1.5%, the sediment primarily consisted of very fine, dispersed, and structurally incoherent particles, indicating substantial inhibition of crystal development due to limited ionic mobility in the solution. Finally, at 2%, the sediment appeared entirely powdery, soft, and devoid of any defined crystal structure, suggesting near-complete suppression of nucleation and crystal growth. This progression clearly demonstrates that increasing the concentration of Sika® ViscoCrete® 111P continuously reduces crystallization

potential, structural integrity, and the volume of crystalline sediment, confirming its role as an effective inhibitor of gypsum crystal formation. These qualitative observations are summarized in Tables 4 and 5, which compares crystal morphology, growth behavior, and sediment characteristics at different concentrations of Sika® ViscoCrete® 111P after 12 weeks of crystallization.

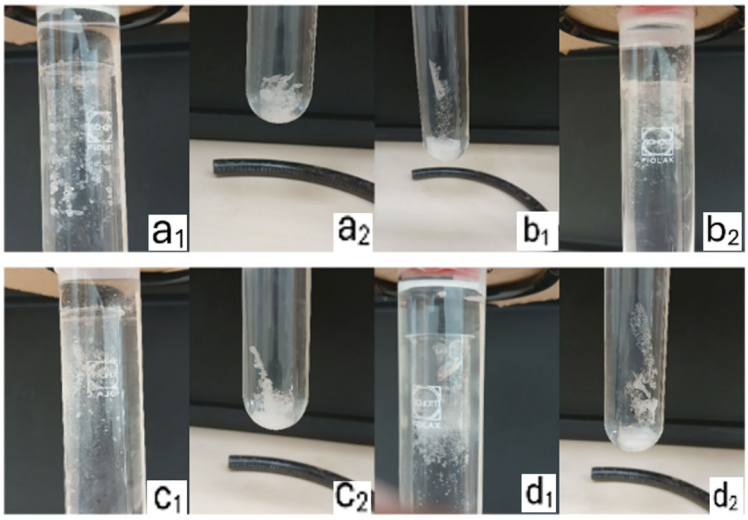

Figure 7. Effect of Sika® ViscoCrete® 111P concentration on gypsum crystallization after 12 weeks: (**a1**,**a2**) 0.5%; (**b1**,**b2**) 1%; (**c1**,**c2**) 1.5%; (**d1**,**d2**) 2%.

Table 4. Summary of observed crystallization stages, crystal morphology, and solution appearance over the 12-week experimental period with Sika® ViscoCrete® 111P addition.

Time	Crystallization Stage	Crystal Observation	Solution Appearance
1st week	Supersaturation (Pre-nucleation)	No visible crystals	Clear and colorless
3rd week	Initial Nucleation	Fine, needle-like crystals starting to form	Slightly cloudy (locally)
4th week	Crystal Growth	Larger and more crystals, radially dispersed	Moderately cloudy
12th week	Saturation and Final Equilibrium	Dense, clustered crystals with fibrous structure	Cloudy and dense

Table 5. Summary of the concentration-dependent effects of Sika® ViscoCrete® 111P on gypsum ($CaSO_4 \cdot 2H_2O$) crystal morphology, growth behavior, and sediment characteristics after 12 weeks.

Concentration (%) of Sika® ViscoCrete® 111P	Crystal Morphology	Growth Behavior	Sediment Characteristics
0.5%	Branched, well-formed, dense	Unrestricted growth, full development	Heavy, settled due to crystal weight
1%	Smaller, compact, less distinct edges	Partially inhibited, moderate diffusion limitation	Compact clusters with some powdery deposits
1.5%	Fine, dispersed, weak structural integrity	Strong inhibition, limited ionic mobility	Light, scattered, filamentous fragments
2%	Powdery, soft, amorphous	Severely inhibited near-complete growth suppression	Soft, fine powder with no defined structure

3.6. Effect of Varying Concentrations of Sika® ViscoCrete® 120P on Early-Stage Gypsum Crystallization in Aqueous Solution

At the fourth week of gypsum ($CaSO_4 \cdot 2H_2O$) crystallization in the presence of different concentrations of the superplasticizer Sika® ViscoCrete® 120P, a clear concentration-dependent effect on the nucleation and early crystal growth process was observed. At 0.5%, small and relatively distinct crystal clusters appeared on the inner wall of the tube, indicating the onset of nucleation under conditions with relatively low diffusion limitation. At 1%, the crystals were fewer, smaller, and more widely dispersed, suggesting the beginning of the inhibitory effect of the superplasticizer on crystal development. At 1.5%, only one or two tiny crystals were visible, reflecting a significant reduction in nucleation rate and a more pronounced restriction of ion mobility in the solution. Finally, at 2%, no visible crystals were observed and the solution remained clear, indicating that nucleation was completely suppressed at this high concentration of Sika® ViscoCrete® 120P. These results demonstrate that increasing concentrations of this superplasticizer effectively control gypsum crystallization by limiting mass transfer and diffusion in the system cf. Figure 8.

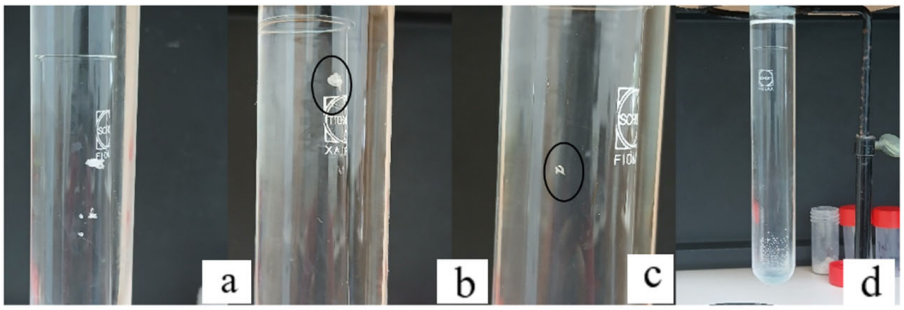

Figure 8. Effect of varying concentrations of Sika® ViscoCrete® 120P on early-stage gypsum ($CaSO_4 \cdot 2H_2O$) crystallization after 4 weeks: (**a**) 0.5%—small, well-defined crystal clusters indicating low inhibition of nucleation; (**b**) 1%—fewer and more dispersed crystals suggesting the onset of diffusion restriction; (**c**) 1.5%—one or two isolated microcrystals reflecting significant nucleation suppression; (**d**) 2%—no visible crystals, indicating complete inhibition of nucleation due to high superplasticizer concentration. The figure illustrates a clear concentration-dependent regulation of gypsum nucleation and initial crystal growth.

3.7. Concentration-Dependent Effects of Sika® ViscoCrete® 120P on Gypsum Crystal Growth and Morphology After 12 Weeks

Based on the visual observations after 12 weeks of gypsum crystal synthesis (Figure 9) in the presence of SP-120 superplasticizer at varying concentrations, significant differences were noted in crystal formation in the upper regions and sedimentation in the lower parts of the test tubes. At a concentration of 0.5%, crystals formed as large, branched clusters in the upper zone, with some aggregating and settling at the bottom due to their weight and cohesion. This behavior indicates favorable conditions for free crystal growth and effective ionic mobility. At 1%, crystal growth was noticeably reduced; small, less compact crystals appeared both at the top and as light, scattered sediments at the bottom, reflecting a moderate inhibition of growth. At 1.5%, crystal development was clearly disrupted, with irregular and fine particles dispersed in both upper and lower regions, showing substantial suppression of nucleation and growth. Interestingly, at 2%, contrary to the initial assumption of complete inhibition, some crystals were observed adhered to the upper walls of the tube, and a distinct elongated crystal had grown upwards from the base. This suggests that despite the overall suppression, localized conditions still allowed for directional growth. Overall, increasing SP-120 concentration resulted in reduced uniformity, cohesion, and size of the crystals, promoting the dominance of disordered particle sedimentation over structured crystal formation. These qualitative observations are summarized in Tables 6 and 7,

which compares crystal morphology, growth behavior, and sediment characteristics at different concentrations of Sika® ViscoCrete® 111P after 12 weeks of crystallization.

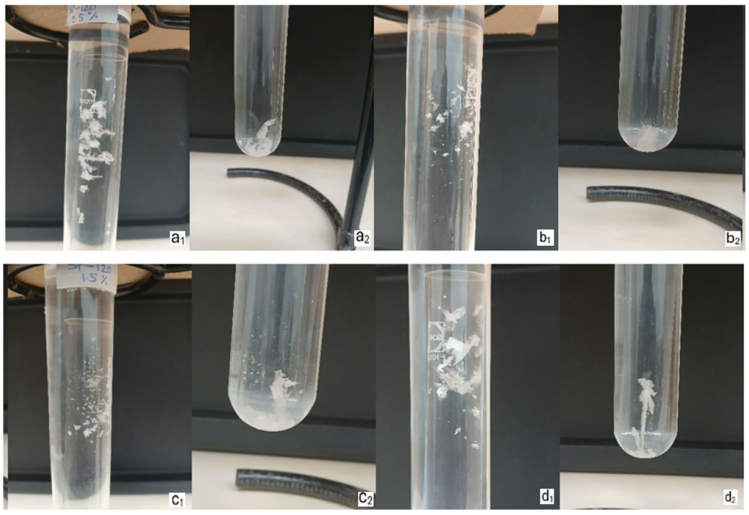

Figure 9. Effect of Sika® ViscoCrete® 120P concentration on gypsum ($CaSO_4 \cdot 2H_2O$) crystallization after 12 weeks: (**a1**,**a2**) 0.5%—large, branched crystals with partial settling; (**b1**,**b2**) 1%—fewer, dispersed crystals showing moderate inhibition; (**c1**,**c2**) 1.5%—fine, irregular particles indicating strong suppression; (**d1**,**d2**) 2%—localized growth with wall-adhered and upward-growing crystals. Crystal size and order decrease with increasing SP-120 concentration.

Table 6. Summary of observed crystallization stages, crystal morphology, and solution appearance over the 12-week experimental period with Sika® ViscoCrete® 120P addition.

Time	Crystallization Stage	Crystal Observation	Solution Appearance
1st week	Supersaturation (Pre-nucleation)	No visible crystals	Clear and colorless
3rd week	Initial Nucleation	Small clusters on inner wall, indicating low inhibition of nucleation	Slightly cloudy (locally)
4th week	Crystal Growth	Fewer or isolated microcrystals at higher concentrations, strong suppression evident	Moderately cloudy
12th week	Saturation and Final Equilibrium	Large branched clusters at 0.5%, irregular/fine at 1.5%, localized growth at 2%	Cloudy or partially clear

Table 7. Summary of the concentration-dependent effects of Sika® ViscoCrete® 120P on gypsum ($CaSO_4 \cdot 2H_2O$) crystal morphology, growth behavior, and sediment characteristics after 12 weeks.

Concentration (%) of Sika® ViscoCrete® 120P	Crystal Morphology	Growth Behavior	Sediment Characteristics
0.5%	Distinct, large, transparent, well-formed	Minimal inhibition, unrestricted growth	Distributed, heavy settled crystals
1%	Dense aggregates adhering to wall	Moderate inhibition, limited volumetric growth	Compact clusters, wall-adhered
1.5%	Smaller, rounded, sparsely distributed	Noticeable inhibition, reduced growth rate	Sparse, light fragments
2%	Fine, irregular, highly clustered	Strong suppression of nucleation and growth	Fine, soft powder-like clusters

3.7.1. Effect of Superplasticizer Type and Dosage on Crystal Nucleation and Growth

In the reference system without any additive, the solution remained clear during the first two weeks. Distinct needle-like crystals were visibly observed by week 3. In all three superplasticizers (SP-430, SP-111, and SP-120), at the first three dosages (0.5%, 1.0%, and 1.5% *w*/*w*), the first visible crystals appeared in week 4. However, the extent of growth and the number of crystals decreased with increasing dosage. For SP-430 at 0.5%, reduced growth and fewer crystals were observed. In contrast, at higher dosages (1.0% and 1.5%), the growth was significantly less, and only sparse crystals were detected, and at 2.0% minimal growth was evident. For SP-111, a similar trend was observed: the first visible crystals appeared in week 4, but with increasing dosage, the growth and number of crystals decreased. In the case of SP-120, the first visible crystals also appeared in week 4 at the first three dosages, and the extent of growth decreased as the dosage increased; however, at the highest dosage (2.0%), no crystals were observed by week 4, and the first visible crystals appeared only in week 5. These results demonstrate that increasing the superplasticizer dosage reduces crystal growth and delays nucleation, with SP-120 showing the strongest inhibitory effect at the highest dosage. These findings are summarized in Table 8 for clarity.

Table 8. Effect of superplasticizer type and dosage on crystal nucleation and growth.

Superplasticizer	Dosage (% *w*/*w*)	Induction time (week)	Observed crystal growth pattern
Reference (no additive)	—	3	Distinct needle-like crystals observed (Figure 3)
SP-430	0.5	4	Reduced growth, fewer crystals (Figure 4)
SP-430	1.0	4	Significantly less growth, sparse crystals
SP-430	1.5	4	Noticeably less growth, sparse crystals
SP-430	2.0	4	Minimal growth, very few crystals
SP-111	0.5	4	Reduced growth, fewer crystals (Figure 6)
SP-111	1.0	4	Significantly less growth, sparse crystals
SP-111	1.5	4	Noticeably less growth, sparse crystals
SP-111	2.0	4	Minimal growth, very few crystals
SP-120	0.5	4	Reduced growth, fewer crystals (Figure 8)
SP-120	1.0	4	Significantly less growth, sparse crystals
SP-120	1.5	4	Noticeably less growth, sparse crystals
SP-120	2.0	5	No visible crystals up to week 4; first crystals appeared at week 5 (Figure 8)

3.7.2. Mechanistic Comparison of the Inhibitory Performance of the Tested Superplasticizers

The inhibitory effects of the three tested superplasticizers (430P, 111P, and 120P) on gypsum crystallization can be attributed to differences in their molecular structure and functional groups. Each superplasticizer interacts with the growing crystal surfaces through a combination of electrostatic and steric mechanisms, to varying degrees depending on their specific chemical architecture. Among the tested superplasticizers, 120P exhibited the strongest inhibitory effect on gypsum crystallization, which can be rationalized by its molecular features: compared to 430P and 111P, 120P likely contains longer or more densely packed polyether side chains and a higher density of carboxylate groups. The carboxylate groups enhance adsorption onto the active sites of the growing gypsum crystal surfaces through electrostatic interactions, while the longer and more abundant polyether side chains increase steric hindrance, effectively impeding further crystal growth and nucleation. In summary, the comparative analysis highlights the critical role of both the

density of functional groups and the configuration of polymer side chains in determining the extent of crystallization inhibition, with 120P demonstrating the most efficient molecular design among the tested additives. However, it should be emphasized that the proposed crystallization mechanism—based on diffusion versus adsorption processes in the presence of superplasticizers—remains hypothetical. Confirming this mechanism requires further complementary analyses, including viscosity and diffusion coefficient measurements, as well as surface-sensitive characterization techniques. In this regard, our future work aims to employ advanced analytical methods such as adsorption isotherm measurements, surface spectroscopy (e.g., XPS and FTIR-ATR), time-of-flight secondary ion mass spectrometry (TOF-SIMS), and atomic force microscopy (AFM), to directly investigate the crystal–additive interfacial interactions and further validate the proposed mechanism.

3.8. XRD Analysis of Reference Gypsum Crystals

X-ray diffraction (XRD) analysis was performed on the reference gypsum crystals to confirm their phase composition. The obtained diffraction pattern exhibited sharp and well-defined peaks that are in excellent agreement with the standard reference pattern for gypsum ($CaSO_4 \cdot 2H_2O$), indicating high crystallinity and phase purity. No additional peaks corresponding to other calcium sulfate phases were observed. This confirms that the crystals formed under the applied conditions consist predominantly of pure gypsum, supporting the interpretations drawn from thermal analysis and crystal growth observations cf. Figure 10.

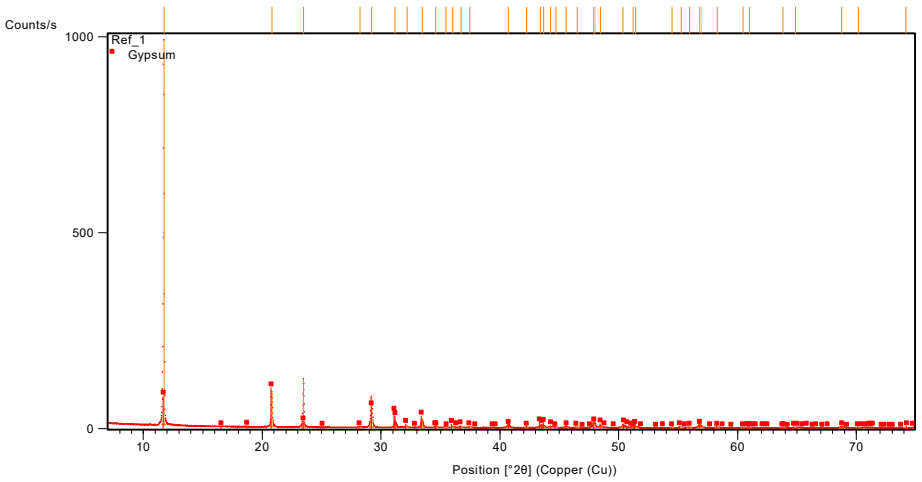

Figure 10. X-ray diffraction (XRD) pattern of the reference gypsum crystals. The diffraction peaks correspond to the standard pattern of gypsum ($CaSO_4 \cdot 2H_2O$), confirming phase purity and high crystallinity. No secondary phases were detected.

3.9. Influence of Superplasticizer on the Surface Microstructure of Synthesized Crystals of Gypsum

The influence of superplasticizers on the crystallization behavior of gypsum was investigated by synthesizing samples with three types of Sika® ViscoCrete® superplasticizers (430P, 111P, and 120) at concentrations of 0.5%, 1%, 1.5%, and 2%. A reference sample without any additive was also included for comparison. Scanning Electron Microscopy (SEM) was employed to characterize changes in crystal morphology.

3.9.1. Morphology of Gypsum Crystals Formed by Diffusion in the Absence of Superplasticizers

The gypsum crystals synthesized via diffusion in the absence of any superplasticizer, after 12 weeks, exhibit a distinct acicular (needle-like) morphology cf. Figure 11. These elongated, narrow, and sharp structures are characteristic of natural crystal growth in a saturated environment and are primarily attributed to rapid nucleation and random crystal

development. The crystals appear densely packed with minimal spacing between them, often showing overlapping and interlocking arrangements, indicative of uncontrolled growth and a high nucleation rate. Their growth direction is random and lacks any specific alignment, suggesting that crystallization occurred freely without any physical or chemical constraints. Moreover, the crystal boundaries are generally indistinct or merged, which can be explained by the high density and simultaneous growth within localized regions. The overall structure is highly compact, leaving virtually no voids between particles. Such microstructural compactness may lead to reduced permeability and increased brittleness in the final gypsum-based material.

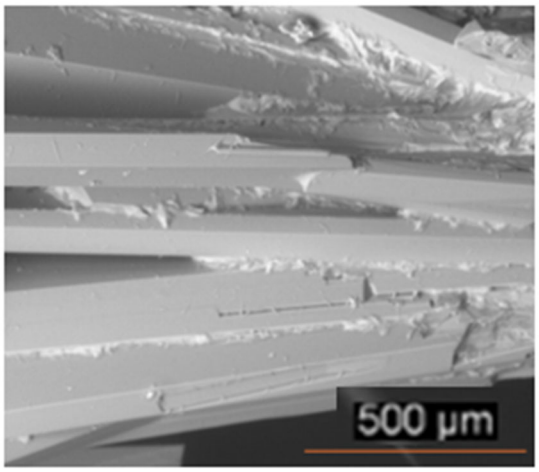

Figure 11. SEM image of gypsum ($CaSO_4 \cdot 2H_2O$) crystals formed by diffusion after 12 weeks in the absence of superplasticizers. The crystals exhibit a dense, acicular (needle-like) morphology with random orientation, interlocking growth, and minimal spacing—indicative of rapid nucleation and unconstrained crystal development.

3.9.2. SEM Characterization of Gypsum Crystallization Behavior Under Varying Concentrations of Sika® ViscoCrete® 430P

The scanning electron microscopy (SEM) images of gypsum crystals ($CaSO_4 \cdot 2H_2O$) synthesized in the presence of 0.5% Sika® ViscoCrete® 430P superplasticizer exhibit a platy, layered, and well-organized morphology. In these images, the crystals have grown as thin, parallel sheets with clear alignment, indicating directional and controlled growth along specific crystallographic planes. In this sample, the presence of the superplasticizer and the slow diffusion of ions through the medium have contributed to a gradual and orderly crystal growth process. As a result, an open and spatially organized structure with minimal compaction has formed, which may predict improved uniformity, controlled porosity, and more stable mechanical behavior in the final gypsum-based material. These morphological characteristics are summarized in Table 9, highlighting the clear edges, high alignment, and low structural density associated with this concentration. A comparison of the SEM images in Figure 12 for the 0.5% and 1% superplasticizer samples reveals notable morphological differences in the gypsum crystals. In the 0.5% sample, the crystals predominantly exhibit a thin, flat, and aligned platy structure, forming orderly, layered arrangements. In contrast, the 1% sample shows a shift toward a thicker, more acicular morphology with a tendency toward prismatic forms. The crystals appear more elongated and thicker, with a semi-ordered orientation. While some crystals align along a dominant axis, angular deviations are also observed, indicating a reduction in directional uniformity compared to the 0.5% sample. Additionally, the crystal density in the 1% sample has slightly increased, with more frequent contact and overlap among the crystals. Nonetheless, their boundaries remain relatively distinct, and the overall structure is still open and

moderately organized. This comparison suggests that increasing the superplasticizer concentration from 0.5% to 1% reduces the nucleation rate and leads to the growth of larger and thicker crystals. The SEM image of the gypsum crystals synthesized with 1.5% Sika® ViscoCrete® 430P reveals a well-developed prismatic morphology. The crystals appear as thick, elongated blades with clearly defined edges and smoother surfaces compared to the lower concentrations. A noticeable increase in crystal size is evident, indicating enhanced individual growth due to a further reduction in nucleation rate. The crystals exhibit relatively consistent orientation, showing more directional alignment than observed at 1%. In contrast to the 0.5% sample, where the morphology was predominantly platy and layered, and the 1% sample, which featured semi-ordered, thicker acicular forms, the 1.5% sample demonstrates a more open, well-separated structure with minimal overlap among crystals. The inter-crystalline spacing has increased, and the compactness has decreased, resulting in clearer boundaries and more distinct crystal forms. This progression suggests that increasing the superplasticizer concentration to 1.5% promotes more controlled and isolated crystal growth, transitioning from layered to prismatic forms, and enhancing both structural definition and spatial regularity. The SEM image of the gypsum sample synthesized with 2% Sika® ViscoCrete® 430P reveals a markedly different morphology compared to the lower concentrations. The crystals exhibit a dense, massive, and somewhat lobular structure, with surfaces that appear irregular and compact. Unlike the more defined prismatic morphology observed at 1.5%, the crystals here are poorly separated, and their boundaries are largely indistinct. The overall texture suggests a high degree of crystal intergrowth and aggregation. No dominant orientation is observed, indicating the loss of directional growth that was evident at 0.5%, 1%, and especially 1.5%. This suggests that at 2% concentration, the superplasticizer may have excessively suppressed the nucleation and growth rates, disrupting the formation of well-defined individual crystals and instead promoting bulk crystallization in a disordered manner. Compared to the lower dosages, which showed a progression from platy to prismatic structures with increasing clarity and separation, the 2% sample reverses this trend—resulting in a compact, merged, and less organized crystal network. This indicates that while moderate amounts of superplasticizer enhance microstructural regularity, excessive levels may hinder crystalline order and lead to undesirable densification. This reversal in crystal definition and increase in structural densification is consistent with the lowest scores for alignment, spacing, and boundary clarity shown in Figure 13.

Table 9. Increasing Sika® ViscoCrete® 430P concentration alters gypsum crystal morphology—from thin, aligned structures at low dosages to bulky, disordered forms at higher levels, reflecting a shift from controlled to inhibited growth.

Superplasticizer Concentration (%)	Dominant Morphology	Crystal Surface Features	Crystal Boundaries	Orientation and Order	Structural Density
0.5%	Thin, platy, layered	Smooth, aligned, clean edges	Clearly defined	Highly aligned	Low
1.0%	Thicker, acicular-prismatic	Slightly rough with intersecting lines	Slight overlap	Semi-aligned with deviations	Moderate
1.5%	Well-defined prismatic	Smooth surfaces, sharp edges	Well-separated	More directional and organized	Low-to moderate
2.0%	Bulky, aggregated, lobular	Rough, irregular, textured	Merged, indistinct	Disordered and random	High (compact)

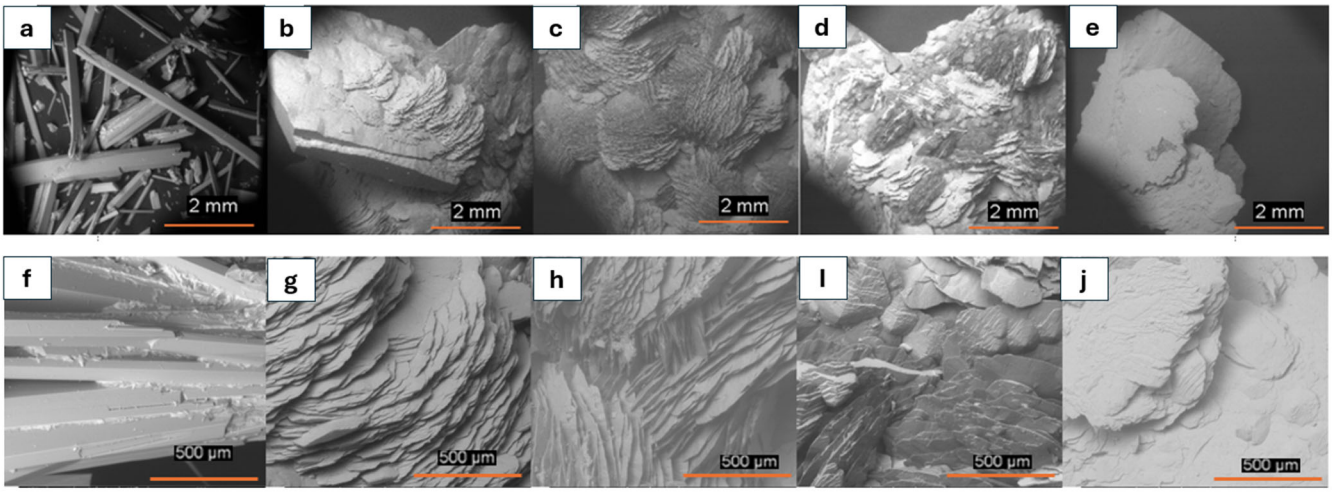

Figure 12. Combined SEM images of gypsum crystals formed in the presence of Sika® ViscoCrete® 430P at different dosages: (**a**–**e**) low-magnification views showing morphological evolution from dense, randomly oriented needle-like crystals (reference) to thin, layered plates (0.5%), thicker prismatic forms (1.0%), well-separated prisms (1.5%), and finally compact, lobular aggregates (2.0%); (**f**–**j**) corresponding high-magnification views revealing microstructural details and progressive densification with increasing dosage. Scale bars: 2 mm for (**a**–**e**), 500 µm for (**f**–**j**).

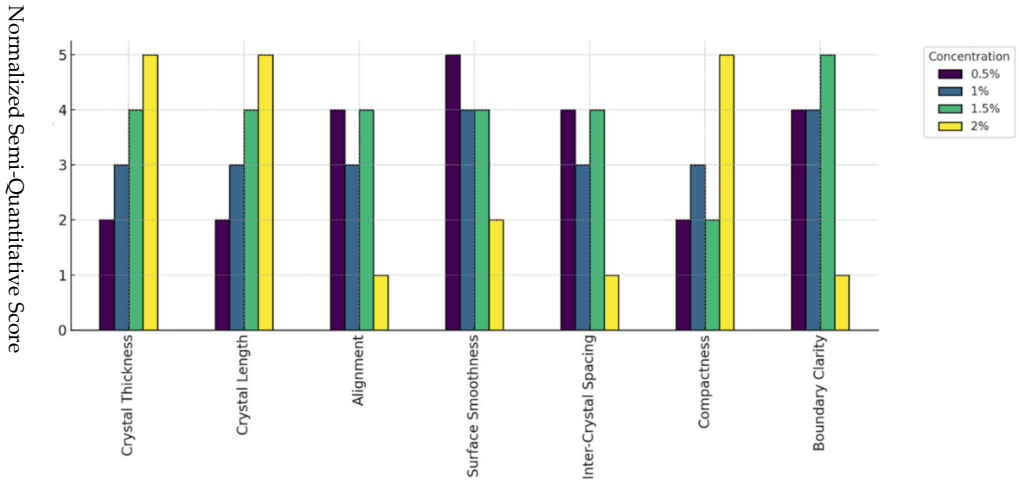

Figure 13. Quantitative comparison of gypsum crystal properties at different concentrations of Sika® ViscoCrete® 430P. The vertical axis (1–5) represents a normalized scale based on semi-quantitative scoring from image analysis. With increasing concentration from 0.5% to 2%, crystal thickness and length increase, while alignment, surface smoothness, inter-crystal spacing, and boundary clarity progressively decrease. The 2% sample shows the highest compactness and lowest structural order, indicating dense but disordered crystal growth. These trends confirm the morphological transition observed in SEM images, highlighting the concentration-dependent impact of the superplasticizer on crystal formation.

3.9.3. SEM Characterization of Gypsum Crystallization Behavior Under Varying Concentrations of Sika® ViscoCrete® 111P

The scanning electron microscopy (SEM) images of gypsum crystals ($CaSO_4 \cdot 2H_2O$) synthesized in the presence of 0.5% Sika® ViscoCrete® 111P superplasticizer shown in Figure 14, exhibit a well-formed prismatic morphology accompanied by local rosette-like structures, particularly at the crystal tips. These formations suggest secondary nucleation at later growth stages, potentially due to localized supersaturation. Despite these irregularities, the main crystal bodies remain geometrically defined and show relatively consistent alignment, indicating partially directional and controlled growth. A comparison

between the 0.5% and 1% samples reveals a noticeable transition in morphology. At 1%, the crystals are larger, smoother, and more elongated with sharper edges and minimal secondary structures. The boundaries are more distinct, and the crystals are well-separated, reflecting reduced nucleation density and enhanced growth of individual crystals in a more anisotropic and ordered fashion. Inter-crystalline spacing increases while overlap is reduced, suggesting further improvement in structural regularity. In the 1.5% sample, the crystals reach a highly developed prismatic form with consistent orientation and minimal surface defects. The morphology appears optimized: crystal size is maximized, edges are clean, and the arrangement is compact yet well-defined. The uniformity and clarity of the crystal network indicate dominant unidirectional growth and minimal random nucleation, representing the most regular and orderly structure among all samples. However, at 2%, a slight deviation from this optimal morphology is observed. While the prismatic form is generally retained, partial merging and aggregation of crystals become apparent in some regions. Boundaries are still visible but less sharp than in the 1.5% sample, and crystal orientation becomes more varied. These observations imply that excessive superplasticizer concentration may begin to interfere with ideal crystal separation and growth dynamics, resulting in a partially dense and less-uniform structure. Overall, increasing the concentration of Sika® ViscoCrete® 111P from 0.5% to 1.5% enhances crystal definition, spacing, and order, with 1.5% appearing to be the optimal dosage. The 2% sample, however, indicates the onset of oversaturation effects, where microstructural regularity begins to decline due to suppressed or disrupted growth behavior. (as summarized in Table 10 and illustrated in Figure 15).

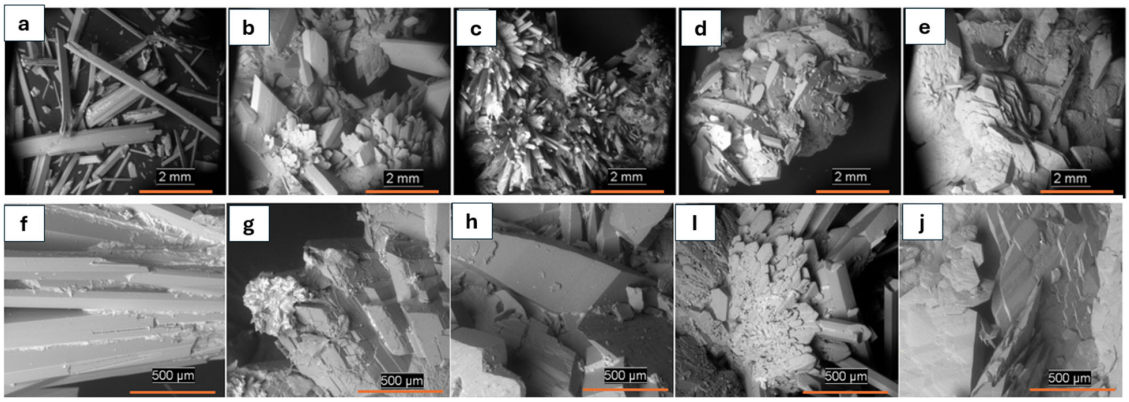

Figure 14. Combined SEM images of gypsum crystals formed in the presence of Sika® ViscoCrete® 111P at different dosages: (**a**–**e**) low-magnification views showing the evolution from prismatic crystals with rosette-like formations (reference) to smoother, elongated and aligned prismatic crystals (0.5–1.0%), partially aggregated crystals with reduced boundary clarity (1.5%), and compact, indistinct aggregates (2.0%); (**f**–**j**) corresponding high-magnification views highlighting microstructural changes, including surface roughness, aggregation, and morphological irregularities with increasing dosage. Scale bars: 2 mm for (**a**–**e**), 500 µm for (**f**–**j**).

Table 10. Summary of gypsum ($CaSO_4 \cdot 2H_2O$) crystal characteristics under varying concentrations of Sika® ViscoCrete® 111P. Increasing the superplasticizer dosage from 0.5% to 1.5% enhances crystal definition, orientation, and separation, with 1.5% yielding prismatic crystals with optimized morphology. At 2.0%, structural irregularities such as merged boundaries, chaotic orientation, and high density emerge, indicating reduced growth control and the onset of oversaturation effects.

Superplasticizer Concentration (%)	Dominant Morphology	Crystal Surface Features	Crystal Boundaries	Orientation and Order	Structural Density
0.5%	Thin, layered, semi-organized	Smooth and clean	Mostly distinct	Semi-aligned with parallel growth	Moderate

Table 10. *Cont.*

Superplasticizer Concentration (%)	Dominant Morphology	Crystal Surface Features	Crystal Boundaries	Orientation and Order	Structural Density
1.0%	Thicker blades, semi-prismatic	Slightly rough, minor secondary growth	Partially overlapping	Moderate alignment, more deviations	Moderate to high
1.5%	Prismatic, irregular tips	Moderately rough with irregular edges	Poorly defined	Less directional growth	High
2.0%	Bulky, dense, disordered	Textured, with merged surfaces	Largely merged	Chaotic and random	Very high

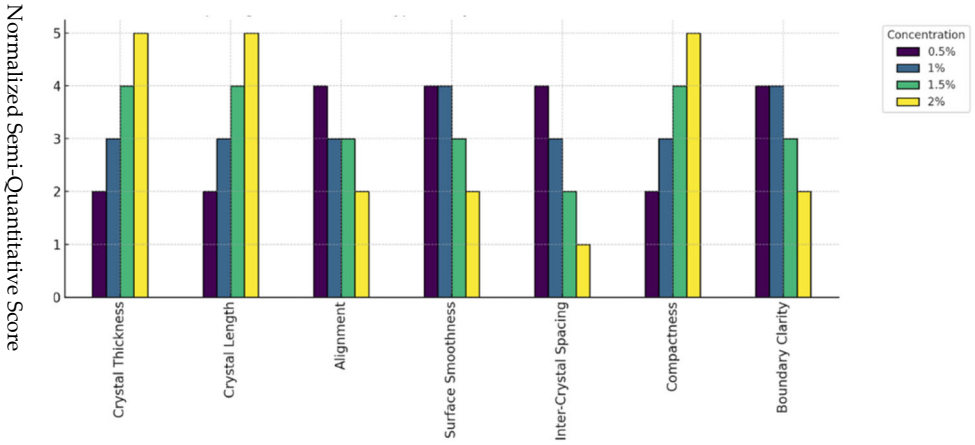

Figure 15. Quantitative comparison of gypsum crystal properties under different concentrations of Sika® ViscoCrete® 111P, The vertical axis (1–5) represents a normalized scale based on semi-quantitative scoring from image analysis. crystal thickness and length rise steadily, while alignment, surface smoothness, inter-crystal spacing, and boundary clarity decline. Compactness peaks at 2%, indicating denser but less organized structures at higher superplasticizer dosages.

3.9.4. SEM Characterization of Gypsum Crystallization Behavior Under Varying Concentrations of Sika® ViscoCrete® 120P

The SEM image of the gypsum sample synthesized with 0.5% Sika® ViscoCrete® 120 displays a highly ordered platy morphology. The crystals appear as thin, parallel sheets with smooth surfaces and well-defined edges, indicating directional growth along specific crystallographic planes. The layered structure is compact yet well-separated, and no secondary growths or surface deposits are visible. These characteristics suggest a low nucleation rate and gradual, controlled crystal development. At 1% concentration, the crystals retain their platy character but become noticeably thicker. Slight angular deviations are observed in the alignment of the layers, and some overlap between crystals begins to occur. The surfaces remain relatively clean but show faint intersecting growth lines, hinting at moderate variations in the local growth environment. The overall morphology remains fairly ordered, though slightly less uniform than at 0.5%. With 1.5% superplasticizer, a distinct morphological shift is observed. Crystals exhibit fan-like or leaf-shaped structures with a less-consistent orientation. Their surfaces appear partially covered with fine-grained residues, suggesting an increase in secondary nucleation or disturbed crystallization conditions. The spacing between crystals is reduced, and the overall structure becomes more irregular and loosely organized. At 2%, the morphology deteriorates further. The crystals appear bulky, aggregated, and heavily textured. Their surfaces are rough, and clear boundaries are largely absent. A significant degree of crystal intergrowth and

structural compactness is observed. This change implies that the high concentration of superplasticizer may have excessively suppressed the natural crystallization process, leading to chaotic, uncontrolled crystal growth. So, as the concentration of Sika® ViscoCrete® 120 increases from 0.5% to 2%, a progressive loss of structural clarity, alignment, and separation is evident. The 0.5% and 1% samples show well-developed platy morphologies with directional growth, while higher concentrations (especially at 2%) result in disordered, compact structures with poor definition cf. Figure 16. This indicates that moderate concentrations (0.5–1%) are optimal for promoting controlled crystallization, whereas excessive amounts disrupt the growth dynamics and reduce microstructural quality (as shown in Table 11 and illustrated in Figure 17).

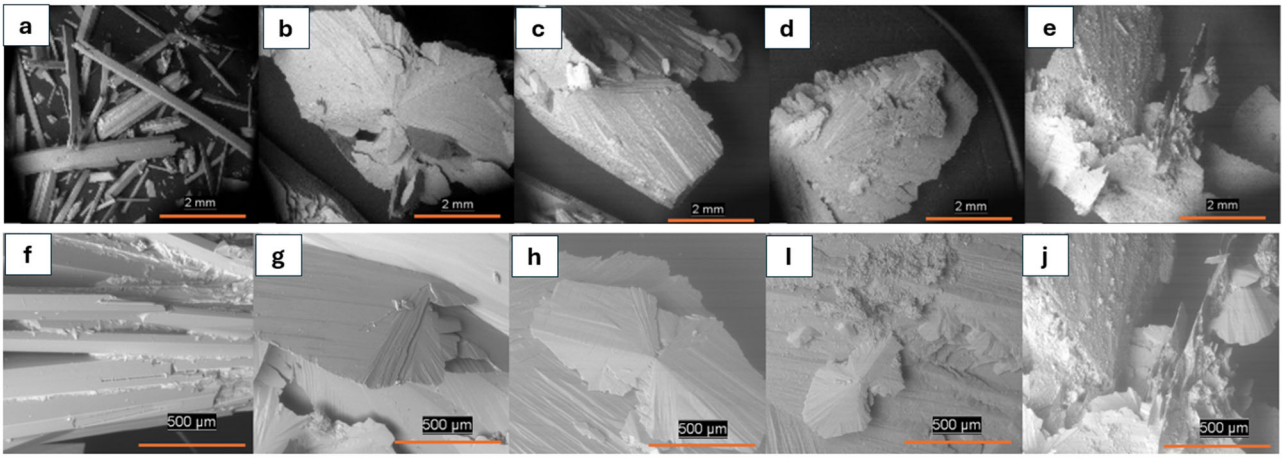

Figure 16. Combined SEM images of gypsum crystals formed in the presence of Sika® ViscoCrete® 120P at different dosages: (**a**–**e**) low-magnification views illustrating the morphological evolution from acicular crystals (reference) to smooth, aligned platy sheets (0.5%), thicker plates with slight misalignment (1.0%), fan-like irregular forms (1.5%), and bulky, merged aggregates (2.0%); (**f**–**j**) corresponding high-magnification views confirming microstructural details, progressive loss of alignment, increased disorder, and aggregation as the dosage increases. Scale bars: 2 mm for (**a**–**e**), 500 µm for (**f**–**j**).

Table 11. Summary of gypsum crystal characteristics under different concentrations of Sika® ViscoCrete® 120. Increasing dosage from 0.5% to 2.0% leads to a transition from well-organized, thin platy crystals with smooth surfaces and clear boundaries to bulky, disordered forms with rough textures and merged edges. Orientation and structural order decline, while density and aggregation increase at higher concentrations.

Superplasticizer Concentration (%)	Dominant Morphology	Crystal Surface Features	Crystal Boundaries	Orientation and Order	Structural Density
0.5%	Thin, platy, well-organized	Smooth, clean, no secondary deposits	Clearly defined	Highly aligned and directional	Low (open structure)
1.0%	Thicker platy	Smooth with slight intersecting lines	Well-defined, slight overlap	Mostly aligned, slight deviation	Moderate
1.5%	Fan-like leaf-like	Covered with fine particles	Less distinguishable	Loss of consistent orientation	Relatively high
2.0%	Bulky and disordered	Rough, textured	Poorly defined or merged	No dominant orientation	High (compact structure)

These microstructural and thermal differences are expected to influence the macroscopic properties of the hardened gypsum plaster. According to reports in the scientific literature, larger and more ordered crystals (typically formed at lower superplasticizer dosages) tend to produce a more open and porous microstructure, which can lead to re-

duced mechanical strength but improved thermal resistance due to lower density and higher permeability. In contrast, fine and densely packed microcrystals (formed at higher dosages) are associated with a denser microstructure that enhances mechanical strength, although it may slightly reduce thermal insulation performance. Therefore, controlling the superplasticizer dosage allows for tuning the balance between strength and thermal behavior of the hardened gypsum plaster depending on the intended application.

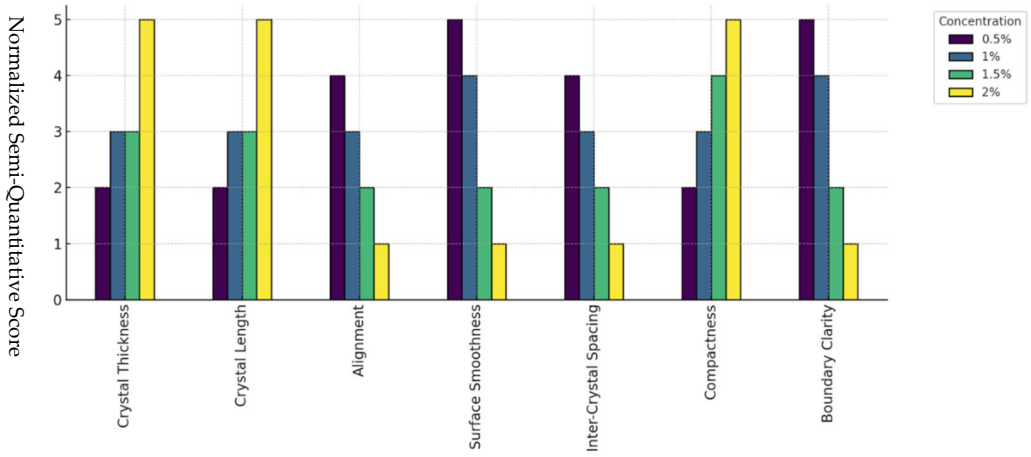

Figure 17. Quantitative comparison of gypsum crystal properties under different concentrations of Sika® ViscoCrete® 120. The vertical axis (1–5) represents a normalized scale based on semi-quantitative scoring from image analysis. With increasing dosage, crystal thickness and compactness rise, while alignment, smoothness, spacing, and boundary clarity progressively decline, indicating a shift from ordered to disordered microstructure.

3.10. Localized Inhibition of Gypsum Crystallization Due to Superplasticizer Accumulation: Evidence from SEM

The SEM image Figure 18 reveals a central, non-crystalline zone disrupting the otherwise prismatic gypsum crystal matrix. This irregular band likely results from localized superplasticizer accumulation, which inhibited nucleation and suppressed crystal growth. Such localized accumulation appears to stem from the inherent tendency of the superplasticizer to distribute unevenly during crystallization, rather than being solely an experimental artifact. The directional growth of crystals on both sides of the band indicates that two growth fronts were obstructed upon encountering the polymer-rich region. This morphological discontinuity underscores the importance of achieving a more uniform dispersion of the superplasticizer during synthesis in order to minimize heterogeneities and ensure consistent crystal growth.

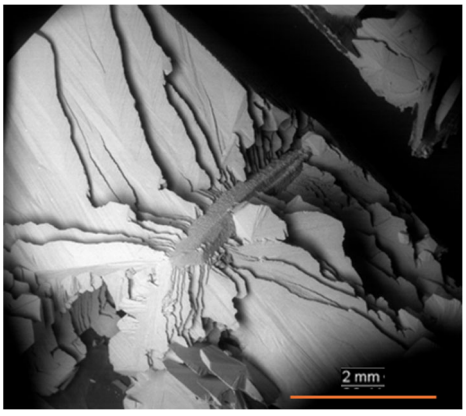

Figure 18. SEM image showing a central non-crystalline band in gypsum, likely caused by local superplasticizer accumulation disrupting crystal growth and alignment.

3.10.1. Effect of Sika® ViscoCrete® 430P Concentration on the Thermal Behavior of Gypsum Crystals (TG Analysis)

The thermogravimetric (TG) analysis of gypsum crystals synthesized with different concentrations of the superplasticizer Sika® ViscoCrete® 430P reveals a clear concentration-dependent effect on water content and crystal structure illustrated in Figure 19a,b. The highest mass loss was observed in the sample containing 0.5% SP-430 (21.01%), suggesting enhanced incorporation of structural water or a more open crystalline network that facilitates thermal release. In contrast, the reference sample (no additive) showed the lowest mass loss (19.12%), indicating a denser, more stable crystalline framework with lower water retention. Samples with 1.5% and 2% SP-430 exhibited intermediate mass losses of 20.50% and 19.93%, respectively, while the 1% sample showed 19.37%, slightly higher than the reference. These results demonstrate that low concentrations of SP-430 promote water integration and potentially more porous crystal formation, whereas higher concentrations reduce crystallinity or restrict water incorporation, leading to more compact and thermally stable structures.

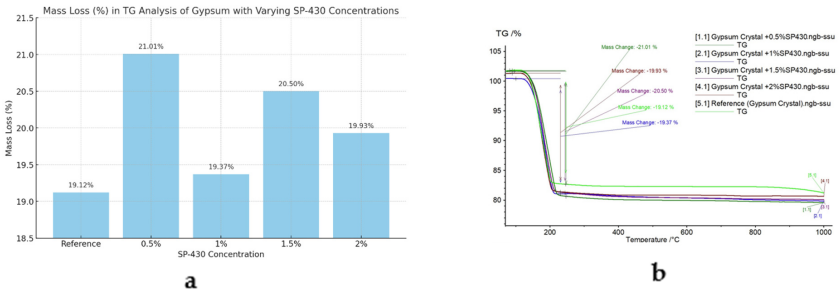

Figure 19. (**a**) TG analysis of mass loss in gypsum crystals with varying concentrations of Sika® ViscoCrete® 430P. (**b**) Thermogravimetric (TG) curves of gypsum crystals synthesized with various concentrations of Sika® ViscoCrete® 430P (0.5%, 1%, 1.5%, and 2%) compared to the reference sample without superplasticizer. The curves correspond to reference (light green), 0.5% (black), 1% (blue), 1.5% (purple), and 2% (red).

3.10.2. Differential Scanning Calorimetry Investigation of Gypsum Crystals Synthesized with SP-430 Superplasticizer

The DSC analysis of gypsum crystals synthesized with varying concentrations of SP-430 superplasticizer revealed significant differences in thermal behavior shown in Figure 20a,b. The main endothermic peak, occurring between approximately 140 °C and 200 °C, corresponds to the dehydration process of gypsum ($CaSO_4 \cdot 2H_2O \rightarrow CaSO_4 \cdot ½H_2O + H_2O$). The enthalpy values derived from the peak areas indicated that the 0.5% SP-430 sample exhibited the highest energy absorption (573.5 J/g), followed by the 1.5% sample (548.8 J/g), while the reference (no additive) showed 533.7 J/g. In contrast, higher concentrations such as 1% and 2% resulted in reduced energy uptake, measured at 527.5 J/g and 521 J/g, respectively. Additionally, the endothermic peak temperatures of the 1% and 2% samples shifted to lower values compared to the reference, whereas those of the 0.5% and 1.5% samples remained similar or slightly higher. These findings suggest a dual effect of SP-430: at low concentrations, it promotes more orderly crystal structures and enhances thermal stability; at higher concentrations, it likely disrupts the crystalline network or traps water in weaker sites, resulting in premature dehydration and reduced thermal energy absorption. Moreover, in the exothermic region of the DSC curves (approximately 350 °C to 800 °C), all samples displayed minor to moderate heat release, which is likely associated with structural rearrangements or degradation of residual organic components. It is plausible that both mechanisms—lattice reorganization at high temperatures and thermal breakdown of adsorbed superplasticizer molecules—contribute to the observed exothermic signals to varying extents depending on concentration. Notably, the 2% SP-430 sample exhibited the

highest exothermic enthalpy change (−0.74 J/g), indicating greater structural transformations at high temperature, while the 1.5% sample showed the lowest exothermic signal (−1.408 J/g), suggesting higher thermal stability. The reference sample released −5.852 J/g, placing it in the intermediate range. These thermal behaviors underscore the significant influence of SP-430 concentration on both dehydration dynamics and high-temperature transformations of gypsum crystals.

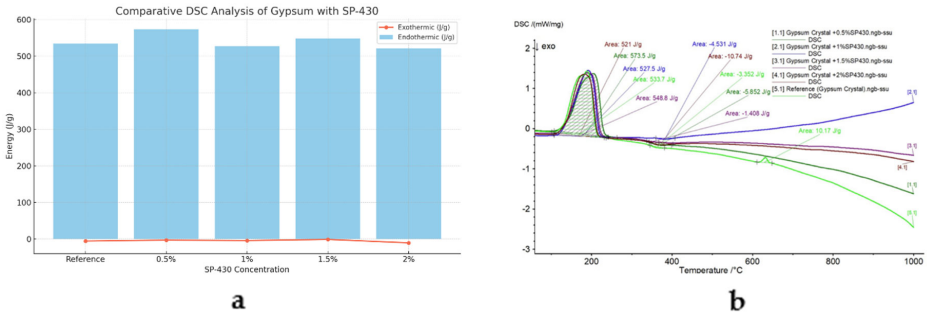

Figure 20. (**a**) Comparison of endothermic and exothermic energies in gypsum crystals with different SP-430 superplasticizer concentrations based on DSC analysis. (**b**) Differential scanning calorimetry (DSC) curves of gypsum crystals synthesized with various concentrations of Sika® ViscoCrete® 430P (0.5%, 1%, 1.5%, and 2%) compared to the reference sample without superplasticizer. The curves correspond to reference (light green), 0.5% (black), 1% (blue), 1.5% (purple), and 2% (red).

3.10.3. Effect of Sika® ViscoCrete® 111P Concentration on the Thermal Behavior of Gypsum Crystals (TG Analysis)

The second investigated superplasticizer revealed notable variations in mass loss within the temperature range of approximately 100–200 °C, corresponding to the dehydration of crystalline water ($CaSO_4 \cdot 2H_2O \rightarrow CaSO_4 \cdot ½H_2O + H_2O$). The highest mass loss was observed in the 1% SP-111 sample (21.59%), indicating either a higher water content in the crystal lattice or enhanced release capability due to structural modification. This was followed by the 0.5% (21.28%) and 2% (20.03%) samples, all of which showed greater water loss than the reference gypsum crystal (19.12%), implying that SP-111 promotes higher water retention or looser crystal formation as shown in Figure 21a,b. Interestingly, the 1.5% sample demonstrated a relatively lower mass loss (19.72%), which may be attributed to a denser crystalline network or restricted water release. These findings highlight the concentration-dependent dual effect of SP-111 on gypsum crystallization and thermal behavior, with 1% concentration showing the most significant enhancement in structural water release see in Figure 21a,b.

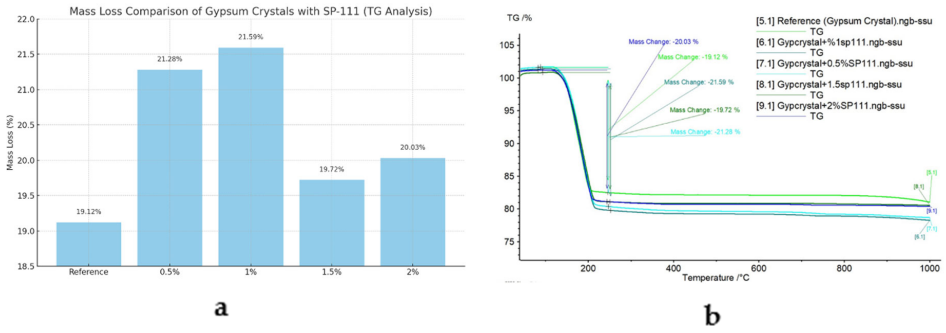

Figure 21. (**a**) Comparison of Endothermic and Exothermic Energies in Gypsum Crystals with Different SP-111 Superplasticizer Concentrations Based on DSC Analysis. (**b**) Thermogravimetric (TG) curves of gypsum crystals synthesized with various concentrations of Sika® ViscoCrete® 111P (0.5%, 1%, 1.5%, and 2%) compared to the reference sample without superplasticizer. The curves correspond to reference (light green), 0.5% (cyan), 1% (blue), 1.5% (dark green), and 2% (dark blue).

3.10.4. Differential Scanning Calorimetry Investigation of Gypsum Crystals Synthesized with SP-111 Superplasticizer

The DSC (Differential Scanning Calorimetry) analysis of gypsum crystals synthesized with varying concentrations of SP-111 superplasticizer reveals notable differences in thermal behavior as illustrated in Figure 22a,b. The highest endothermic energy absorption was recorded in the 0.5% SP-111 sample (598.8 J/g), indicating a more ordered crystalline structure and higher structural water content. This was followed by the 1.5% and 2% samples, which exhibited enthalpy values of 572.2 J/g and 550.1 J/g, respectively. The reference sample without any additive showed a moderate value of 533.8 J/g. In contrast, the 1% SP-111 sample displayed the lowest endothermic peak area at 498.1 J/g, suggesting that this specific concentration may disrupt crystallization and reduce the energy required for dehydration. This non-monotonic trend in crystal stability may arise from competing effects of polymer adsorption and surface coverage at different concentrations. At intermediate concentrations (1 wt %), polymer coverage likely interferes most strongly with the lattice ordering, resulting in the lowest dehydration enthalpy, while at higher concentrations (1.5 wt %), more uniform surface saturation may allow for a slightly more ordered growth. These trends confirm that SP-111 influences gypsum's crystallization and thermal behavior in a concentration-dependent manner—lower concentrations (especially 0.5%) enhance crystallinity and thermal stability, whereas higher concentrations tend to weaken this effect. In the exothermic region of the DSC curve, occurring roughly between 600 °C and 700 °C, exothermic peaks were only observed in the samples containing 0.5%, 1.5%, and 2% SP-111. The corresponding released energies were −1.87 J/g, −6.838 J/g, and −5.969 J/g, respectively. These exothermic responses are likely associated with structural rearrangements or recrystallization events triggered by elevated temperatures. In addition, partial thermal degradation of residual organic superplasticizer components adsorbed on the crystal surfaces may also contribute to the observed exothermic peaks. The most intense exothermic effect was observed in the 1.5% sample, possibly due to the presence of a less stable crystal network prone to thermal decomposition. The absence of exothermic activity in the reference and 1% SP-111 samples suggests that SP-111 at certain concentrations alters the crystal structure in a way that enhances reactivity at high temperatures. Overall, the DSC results indicate that SP-111 not only affects dehydration processes but also modulates the thermal stability and transformation pathways of gypsum under high-temperature conditions.

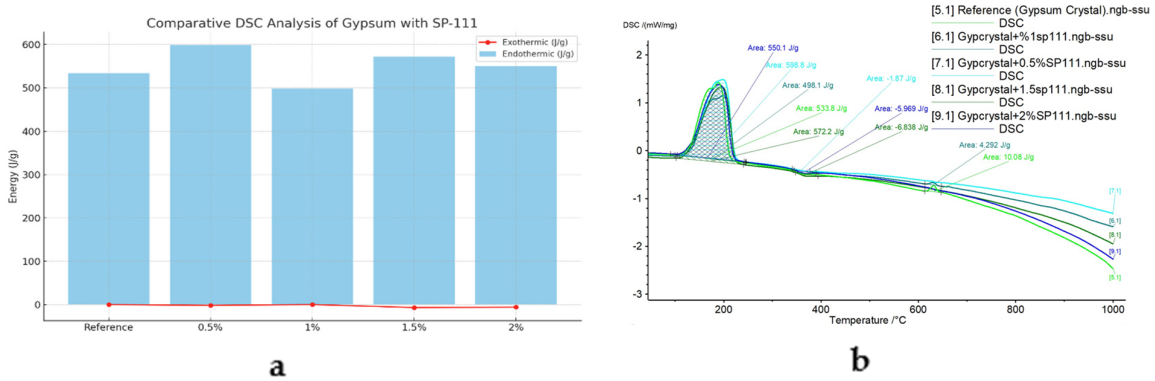

Figure 22. (**a**) Comparison of Endothermic and Exothermic Energies in Gypsum Crystals with Different SP-111 Superplasticizer Concentrations Based on DSC Analysis. (**b**) Differential scanning calorimetry (DSC) curves of gypsum crystals synthesized with various concentrations of Sika® Visco Crete® 111P (0.5%, 1%, 1.5%, and 2%) compared to the reference sample without superplasticizer. The curves correspond to reference (light green), 0.5% (cyan), 1% (blue), 1.5% (dark green), and 2% (dark blue).

3.10.5. Effect of Sika® ViscoCrete® 120P Concentration on the Thermal Behavior of Gypsum Crystals (TG Analysis)

The thermogravimetric (TG) analysis of gypsum crystals synthesized with varying concentrations of SP-120 superplasticizer demonstrates a clear concentration-dependent effect on thermal dehydration behavior as illustrated in Figure 23a,b. The reference sample (without additive) showed the lowest mass loss at 19.12%, suggesting a denser, more thermally stable crystalline structure. With the addition of 0.5% SP-120, mass loss increased slightly to 19.90%, indicating marginal enhancement in water content or release. A more notable increase was observed at 1% and 1.5% SP-120, with mass losses of 20.45% and 20.04%, respectively, reflecting both improved water incorporation and structural modifications facilitating dehydration. The maximum mass loss occurred in the 2% SP-120 sample (20.62%), pointing to a more open or disrupted crystal network capable of holding and releasing greater amounts of structural water. Overall, these findings suggest that SP-120 influences the hydration–dehydration characteristics of gypsum, with higher concentrations enhancing thermal water release, likely due to changes in crystal morphology and porosity.

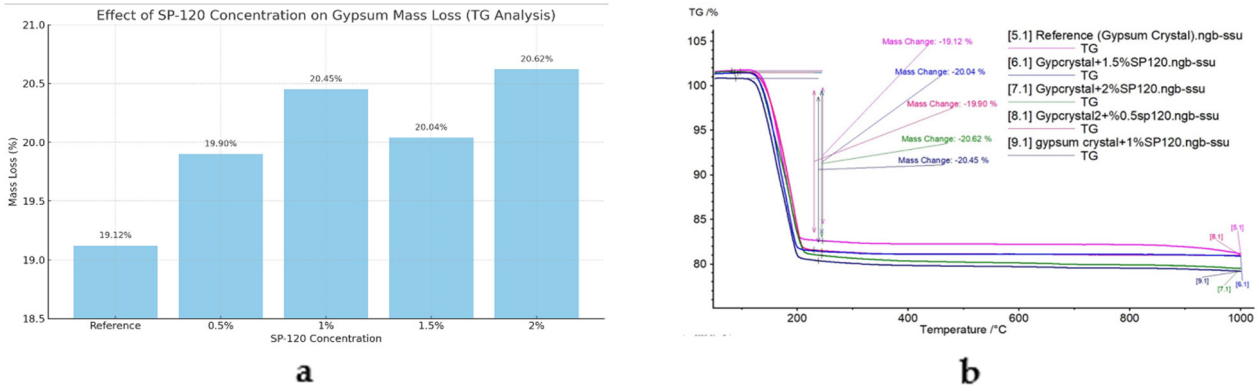

Figure 23. (**a**) Comparison of Endothermic and Exothermic Energies in Gypsum Crystals with Different SP-120 Superplasticizer Concentrations Based on DSC Analysis. (**b**) Thermogravimetric (TG) curves of gypsum crystals synthesized with various concentrations of Sika® ViscoCrete® 120P (0.5%, 1%, 1.5%, and 2%) compared to the reference sample without superplasticizer. The curves correspond to reference (light pink), 0.5% (dark pink), 1% (dark blue), 1.5% (blue), and 2% (green).

3.10.6. Differential Scanning Calorimetry Investigation of Gypsum Crystals Synthesized with SP-120 Superplasticizer

The DSC (Differential Scanning Calorimetry) analysis of gypsum crystals synthesized with varying concentrations of SP-120 superplasticizer reveals significant differences in thermal behavior as illustrated in Figure 24a,b. In the endothermic region, occurring between approximately 100 °C and 200 °C, the highest energy absorption was recorded in the sample containing 1% SP-120 (562 J/g), indicating a more ordered crystalline structure and higher structural water content. The 1.5% and 2% SP-120 samples followed closely with values of 558 J/g and 557.4 J/g, respectively, reflecting consistent thermal performance and structural stability. The 0.5% SP-120 sample also demonstrated a high enthalpy value of 550.7 J/g. In contrast, the reference sample without any additive exhibited the lowest energy uptake (533.7 J/g), suggesting a denser structure with lower thermal responsiveness. These findings indicate that SP-120 enhances the thermal dehydration behavior of gypsum, particularly at the 1% concentration, likely due to improved crystallinity. In the exothermic region, observed between approximately 300 °C and 400 °C, exothermic peaks were detected only in the reference sample (3.352 J/g), the 0.5% SP-120 sample (2.122 J/g), and the 1.5% SP-120 sample (5.19 J/g). These peaks are associated with structural rearrangements or recrystallization processes initiated at elevated temperatures. In addition,

partial thermal degradation of residual organic superplasticizer components adsorbed on the crystal surfaces may also contribute to the observed exothermic heat release. The most pronounced exothermic response was seen in the 1.5% SP-120 sample, possibly indicating a less stable and more reactive crystalline lattice. The absence of exothermic activity in the 1% and 2% SP-120 samples suggests greater structural stability or reduced energy release potential. Overall, these results demonstrate that SP-120 not only influences the dehydration process of gypsum but also alters its thermal stability and high-temperature transformation pathways in a concentration-dependent manner.

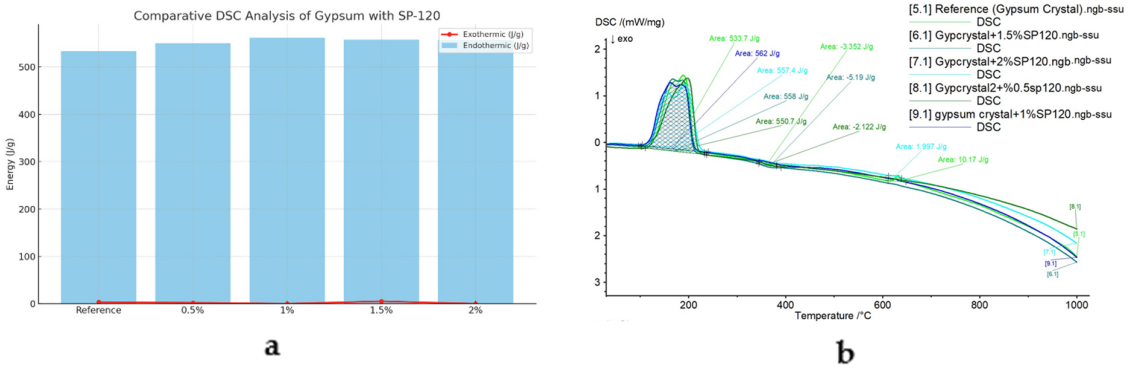

Figure 24. (**a**) Comparison of Endothermic and Exothermic Energies in Gypsum Crystals with Different SP-120 Superplasticizer Concentrations Based on DSC Analysis. (**b**) Differential scanning calorimetry (DSC) curves of gypsum crystals synthesized with various concentrations of Sika® Visco Crete® 120P (0.5%, 1%, 1.5%, and 2%) compared to the reference sample without superplasticizer. The curves correspond to reference (green), 0.5% (dark green), 1% (dark blue), 1.5% (cyan), and 2% (light blue).

3.10.7. Comparative Thermal Analysis of Gypsum Crystals with SP-111, SP-430, and SP-120 at Varying Concentrations

The comparative TGA and DSC analyses of gypsum crystals with SP-111, SP-430, and SP-120 show that both the type and concentration of superplasticizer significantly affect thermal behavior as illustrated in Figure 25a,b. SP-111 led to the highest mass loss at lower concentrations (0.5–1%), while SP-120 had the greatest impact at higher levels (1.5–2%), indicating greater water content or structural openness. In DSC results, 0.5% SP-111 showed the highest energy absorption (598.8 J/g), reflecting high crystallinity and bound water, whereas the lowest value (498.1 J/g) was also from SP-111 at 1%, suggesting structural disruption. SP-430 displayed moderate, stable performance throughout. Overall, thermal responses confirm that optimal effects depend on both formulation and dosage. It should also be noted that despite thorough washing and drying protocols, trace amounts of residual superplasticizer polymer might remain adsorbed on the crystal surfaces, which could slightly bias the thermal behavior observed in TGA/DSC measurements. Therefore, the results of thermal analysis should be interpreted with appropriate caution.

3.11. Correlation Between Crystal Morphology and Thermal Behavior Induced by Superplasticizers

The SEM observations and thermal analysis results are closely correlated, highlighting the link between crystal morphology and thermal behavior of gypsum synthesized with different superplasticizers. SEM images revealed that lower superplasticizer concentrations (e.g., 0.5%) led to well-defined, layered or prismatic crystals with higher structural order and open microstructures, whereas higher concentrations (e.g., 2%) produced denser, aggregated, and disordered crystals. This morphological trend is mirrored in the DSC/TG data, where samples with more ordered microstructures exhibited higher dehydration enthalpies and improved thermal stability, while disordered and compact morphologies at

higher superplasticizer levels showed lower energy absorption, reduced thermal stability, and higher susceptibility to exothermic structural rearrangements or degradation. These findings demonstrate that the degree of crystallinity and the quality of crystal packing, as revealed by SEM, are decisive factors influencing water retention and thermal response of the material.

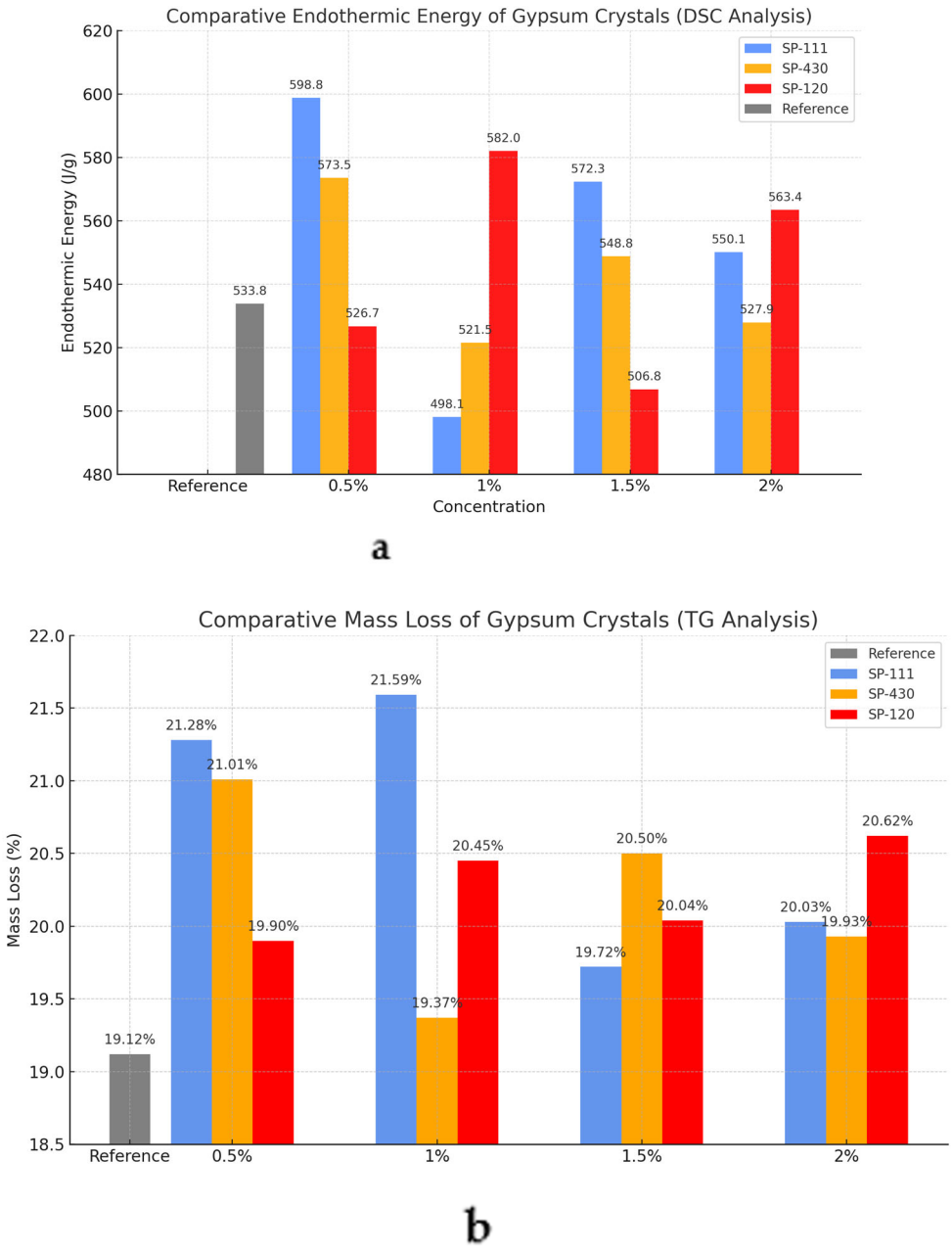

Figure 25. (**a**) Comparison of endothermic enthalpy values (J/g) of gypsum crystals synthesized with different concentrations of three superplasticizers (SP-111, SP-120, and SP-430), as measured by DSC. (**b**) Comparative mass loss analysis of gypsum crystals containing various concentrations of SP-111, SP-430, and SP-120 superplasticizers based on TG measurements.

4. Conclusions

This study investigated the crystallization process of gypsum ($CaSO_4 \cdot 2H_2O$) under controlled diffusion conditions, analyzing the effects of three different superplasticizers from the Sika® ViscoCrete® family—430P, 111P, and 120P—at varying concentrations on crystal growth, morphology, and thermal behavior. The specially designed coaxial test tube system provided a static and undisturbed environment that allowed for natural, structured

crystal formation. Weekly imaging during the crystallization period showed that the addition of superplasticizers delayed the onset of gypsum crystallization. This delay was concentration- and type-dependent, with SP-120 at higher concentrations exhibiting the strongest inhibitory effect on nucleation and crystal growth, while SP-111 at 0.5% concentration facilitated more rapid and orderly growth. These observations highlight the complex and concentration-sensitive influence of superplasticizers on nucleation and crystal development. Scanning Electron Microscopy (SEM) analysis revealed that superplasticizer addition led to significant changes in crystal morphology. The type and dosage of the admixture influenced the shape, size, and packing of the crystals. At lower concentrations (0.5–1%), crystals were more regular and porous, whereas higher concentrations (1.5–2%) resulted in denser, disordered, or even semi-amorphous structures. These morphological changes were consistent with thermal analysis findings, confirming the direct influence of superplasticizers on the structural evolution of gypsum. Thermal analyses (TG/DSC) further demonstrated distinct differences in the thermal behavior of the samples. Lower concentrations led to more ordered crystal structures, higher heat absorption, and reduced dehydration onset temperatures. In contrast, higher concentrations caused the crystal network to become denser or more irregular, facilitating faster structural water release. Overall, this research confirms that superplasticizers not only act as modifiers of crystallization but also serve as engineering tools for tailoring the final structure, thermal response, and microstructure of gypsum. The findings can contribute to optimizing gypsum formulations in industrial, construction, and materials science applications and pave the way for further studies on alternative chemical additives. In the next phase of this research, to gain deeper insight into the molecular mechanisms by which superplasticizers influence the morphology, delay, or inhibition of gypsum crystal growth, it is proposed to employ advanced surface analysis techniques such as TOF-SIMS (Time-of-Flight Secondary Ion Mass Spectrometry), XPS (X-ray Photoelectron Spectroscopy), Raman spectroscopy, and AFM (Atomic Force Microscopy). These methods will enable a detailed examination of surface chemical composition, vibrational characteristics, topography, and spatial distribution of chemical species, providing valuable information on how superplasticizers interact with the crystal surface and modulate crystallization behavior at the nanoscale. These investigations could further clarify the surface-specific interactions driving the observed morphological and thermal changes and help in developing predictive models for additive–crystal interactions in sulfate-based systems.

Author Contributions: Conceptualization, F.K. and C.P.; data curation, F.K., C.P. and T.K.; formal analysis, F.K., C.P. and T.K.; writ-ing—original draft preparation, F.K.; writing—review and editing, C.P. and M.S.K.; supervision, C.P. and M.S.K.; project administration, M.S.K.; funding acquisition, M.S.K. All authors have read and agreed to the published version of the manuscript.

Funding: We confirm that this research received no external funding.

Data Availability Statement: The original contributions presented in this study are included in the article. Further inquiries can be directed to the corresponding authors.

Conflicts of Interest: The authors declare no conflict of interest.

References

1. Abu Zeitoun, E.; Pritzel, C.; Sakalli, Y.; Trettin, R. The Mechanism of the First Hydration-Dehydration Cycle of Pure α- and β-$CaSO_4 \cdot 0.5H_2O$. *Adv. Mater. Sci. Eng.* **2020**, *1*, 1732621. [CrossRef]
2. Pritzel, C.; Emami, M.; Afflerbach, S.; Killian, M.; Trettin, R. Formation of α-Hemihydrate Inside of a Gypsum Crystal During the Dehydration Process. *Crystals* **2022**, *12*, 1780. [CrossRef]
3. Esan, M.T. Review of gypsum reinforced composites as building materials. *Discov. Civ. Eng.* **2024**, *1*, 5. [CrossRef]

4. Luzha, I.; Aliu, B.; Zguro, T. The importance of gypsum in the process of hydration of cement. In Proceedings of the UBT International Conference, Lipjan, Kosovo, 25–27 October 2024.
5. Nicoleau, L.; Van Driessche, A.E.S.; Kellermeier, M. A kinetic analysis of the role of polymers in mineral nucleation: The example of gypsum. *Cem. Concr. Res.* **2019**, *124*, 105837. [CrossRef]
6. Singh, N.B.; Middendorf, B. Calcium sulphate hemihydrate hydration leading to gypsum crystallization. *Prog. Cryst. Growth Charact. Mater.* **2007**, *53*, 57–77. [CrossRef]
7. Krejsová, J.; Kužel, R.; Keppert, M.; Scheinherrová, L.; Vimmrová, A. New insight into the phase changes of gypsum. *Mater. Struct.* **2024**, *57*, 128. [CrossRef]
8. Förthner, S. Kristallisation und Morphologiebeeinflussung bei Gipsen: Untersuchungen zur Steuerung der Makro-Physikalischen Eigenschaften. Doctoral Dissertation, Friedrich-Alexander-Universität Erlangen-Nürnberg, Erlange, Germany, 2011.
9. Abdel-Aal, E.A.; Rashad, M.M. Crystallization of calcium sulfate dihydrate at different supersaturation ratios and different free sulfate concentrations. *Cryst. Res. Technol.* **2004**, *39*, 313–321. [CrossRef]
10. El-Shall, H.; Rashad, M.M.; Abdel-Aal, E.A. Effect of phosphonate additive on crystallization of gypsum in phosphoric and sulfuric acid medium. *Cryst. Res. Technol.* **2002**, *37*, 1264–1273. [CrossRef]
11. Marschetzky, M.; Fischer, H.-B.; Ludwig, H.-M. Superplasticizers in the calcium sulfate system—Plasticizing action and influence on hydration. *ZKG Int.* **2013**, *5*, 159–163.
12. Ma, R.; Wang, Y.; Li, H.; Bai, Y. Progress in the polycarboxylate superplasticizer and their structure-activity relationship—A review. *Mater. Today Commun.* **2023**, *35*, 105838. [CrossRef]
13. Yepes, J.A.F.; Jara, L.M.S.; Gabarrón, A.M.; Alcaraz, A.M.C.; Pérez, J.J. Analysis of additives in gypsum coatings based on melamine, polycarbonate salts, polycarboxylate, and polycarboxylic acids. *Coatings* **2021**, *11*, 1204. [CrossRef]
14. Guo, G.; Gao, G.; Jiang, W.; Wang, X.; Pei, M.; Wang, L. Synthesis of triblock polycarboxylate superplasticizers with well-defined structure and its dispersing performance in β-hemihydrate gypsum. *Molecules* **2023**, *28*, 513. [CrossRef]
15. Fan, L.; Xiong, S.; Wang, W.; Zhang, J.; Zeng, L. Effect of polycarboxylate admixture on the performance of fluorogypsum-based self-leveling material. *Appl. Sci.* **2023**, *13*, 12802. [CrossRef]
16. Guan, B.; Ye, Q.; Zhang, J.; Wu, Z. Interaction between α-calcium sulfate hemihydrate and superplasticizer from the point of adsorption characteristics, hydration and hardening process. *Cem. Concr. Res.* **2010**, *40*, 253–259. [CrossRef]
17. Gao, D.; Zhang, D.; Peng, Y.; Wang, W. Effects of different carboxyl additives on the growth habits of hemihydrate gypsum crystals. *Constr. Build. Mater.* **2022**, *316*, 126037. [CrossRef]
18. Chen, G.; Liu, R.; Song, C.; Luo, J. Preparation of hemihydrate gypsum with controllable morphology in Glycerol–NaCl–Water solutions with maleic acid. *J. Cryst. Growth* **2021**, *576*, 126360. [CrossRef]
19. Li, M.; Wang, Y.; Jiang, H.; Zheng, C.; Guo, Z. Synthesis, characterization and mechanism of polycarboxylate superplasticizer with slump retention capability. *IOP Conf. Ser. Mater. Sci. Eng.* **2017**, *182*, 012036. [CrossRef]
20. Kim, H.; Mohanty, A.K.; Ahn, J.; Tadesse, D.M.; Aswale, S.; Park, S.; Ju, Y.; Paik, H.-j. Microstructure control of acrylic acid-styrenesulfonate copolymers for high-performance gypsum superplasticizers. *Mater. Today Commun.* **2025**, *45*, 112268. [CrossRef]
21. Martins, C.R.; Ruggeri, G.; De Paoli, M.-A. Synthesis in pilot plant scale and physical properties of sulfonated polystyrene. *J. Braz. Chem. Soc.* **2003**, *14*, 797–802. [CrossRef]
22. Kim, H.; Mohanty, A.K.; Lee, S.; Kwon, M.; Chang, T.; Jeon, H.B.; Paik, H.-j. Partially sulfonated polystyrenes: A new gypsum superplasticizer. *Constr. Build. Mater.* **2024**, *418*, 135297. [CrossRef]
23. Cao, W.; Yi, W.; Yin, S.; Peng, J.; Li, J. A novel low-density thermal insulation gypsum reinforced with superplasticizers. *Constr. Build. Mater.* **2021**, *278*, 122421. [CrossRef]
24. Magallanes-Rivera, R.X.; Escalante-García, J.I.; Gorokhovsky, A. Hydration reactions and microstructural characteristics of hemihydrate with citric and malic acid. *Constr. Build. Mater.* **2009**, *23*, 1298–1305. [CrossRef]
25. Silva, D.B.P.; Lima, N.B.; Lima, V.M.E.; Estolano, A.M.L.; Nascimento, H.C.B.; Vilemen, P.; Padron-Hernández, E.; Carneiro, A.M.P.; Lima, N.B.D.; Povoas, Y.V. Producing a gypsum-based self-leveling mortar for subfloor modified by polycarboxylate admixture (PCE). *Constr. Build. Mater.* **2023**, *364*, 130007. [CrossRef]
26. Silva, D.B.P.; Lima, N.B.; Lima, V.M.E.; Estolano, A.M.L.; Nascimento, H.C.B.; Vilemen, P.; Padron-Hernández, E.; Carneiro, A.M.P.; Lima, N.B.D.; Povoas, Y.V. Evaluation of phosphated superplasticizers in high-performance α-calcium sulfate hemihydrate-based floor screeds. *J. Build. Eng.* **2021**, *41*, 102787.
27. Sakthieswaran, N.; Sophia, M. Effect of superplasticizers on the properties of latex modified gypsum plaster. *Constr. Build. Mater.* **2018**, *179*, 675–691. [CrossRef]
28. Abbood, A.A.; Atshan, A.F.; Al-Ridha, A.S.D. Improvement of local gypsum plaster setting time by the combined usage of (TGP) and (PVA) additives. *IOP Conf. Ser. Mater. Sci. Eng.* **2020**, *870*, 012106. [CrossRef]
29. Gou, J.; Li, S.; Jiang, C.; Li, Z.; You, G. A study on the influence of gypsum and $Ca(OH)_2$ on the mechanical properties and hydration behavior of multi-component solid waste-based cementitious materials. *Materials* **2024**, *18*, 1964. [CrossRef] [PubMed]

30. Zhi, Z.; Huang, J.; Guo, Y.; Lu, S.; Ma, B. Effect of chemical admixtures on setting time, fluidity and mechanical properties of phosphorus gypsum based selfleveling mortar. *KSCE J. Civ. Eng.* **2017**, *21*, 1836–1843. [CrossRef]
31. Pan, Y.; Li, H.; Yang, T. Influence of solid waste gypsum and additives on the properties of sulfoaluminate cement-fly ash-gangue ternary binder. *Miner. Metall. Mater.* **2024**, *3*, 7. [CrossRef]
32. Bumanis, G.; Sapata, A.; Sinka, M.; Spurina, E.; Bajare, D. Additive manufacturing of lightweight gypsum and expanded polystyrene granulate composite. *J. Compos. Sci.* **2023**, *7*, 425. [CrossRef]
33. Du, Z.; She, W.; Zuo, W.; Hong, J.; Zhang, Y.; Miao, C. Foamed gypsum composite with heat-resistant admixture under high temperature: Mechanical, thermal and deformation performances. *Cem. Concr. Compos.* **2020**, *108*, 103549. [CrossRef]
34. Feng, C.; Wang, Y.; Wang, L.; Zhao, X.; Zhang, W.; Zhu, J.; Du, M. Improving the water resistance of gypsum-based building materials with slag activated by calcium oxide. *J. CO2 Util.* **2024**, *90*, 102996. [CrossRef]
35. Elert, K.; Spallarossa Jiménez, M.M.; Burgos-Ruiz, M. Gypsum-based materials for exterior applications using lime and recycled pozzolanic additions. *Constr. Build. Mater.* **2024**, *450*, 138713. [CrossRef]
36. Lin, J.; Hui, Y.; Ren, Q.; Xu, H.; Liu, J.; Huang, K.; Ding, Y. Study on hydration properties of composite gypsum: Effect of different forms of soluble phosphorus on the hydration properties of natural hard gypsum composites with hemihydrate gypsum. *Constr. Build. Mater.* **2025**, *490*, 142573. [CrossRef]
37. Peng, W.; Xia, B.; Sha, J.; Shi, R.; Zhang, C.; Xu, W.; Cao, Y.; Wang, W. Preparation of high-strength gypsum by crystal regulation of phosphogypsum in nitrate solution. *J. Am. Ceram. Soc.* **2025**, *108*, e20669. [CrossRef]
38. Pundir, A.; Garg, M.; Singh, R. Evaluation of properties of gypsum plaster-superplasticizer blends of improved performance. *J. Build. Eng.* **2015**, *4*, 100–108. [CrossRef]
39. Pritzel, C.; Kowald, T.; Sakalli, Y.; Trettin, R. *Binding Materials Based on Calcium Sulphates: Composition, Properties, Application*; De Gruyter: Siegen, Germany, 2017.

Disclaimer/Publisher's Note: The statements, opinions and data contained in all publications are solely those of the individual author(s) and contributor(s) and not of MDPI and/or the editor(s). MDPI and/or the editor(s) disclaim responsibility for any injury to people or property resulting from any ideas, methods, instructions or products referred to in the content.